# CHANGES IN CEREBRAL BLOOD VOLUME AND BLOOD FLOW IN BRAIN TUMOURS DURING PROPOFOL OR ISOFLURANE ANAESTHESIA AND HYPERVENTILATION

by

**Aleksa Cenic**

Department of Medical Biophysics

Thesis Submitted in Partial Fulfillment
of the Requirements for the Degree of
Master of Science

Faculty of Graduate Studies
The University of Western Ontario
London, Ontario, CANADA

August 1998

**ABSTRACT**

The effect of hyperventilation on regional cerebral blood volume (CBV) and blood flow (CBF) during Propofol or Isoflurane anaesthesia in brain tumour rabbits was examined. CBV was measured using a previously developed contrast enhanced CT method, while CBF measurements were simultaneously acquired using microspheres. During Propofol, hyperventilation induced a significant decrease in CBV (10%) and CBF (18%) in only the peri-tumour region. During Isoflurane, hyperventilation induced a significant global decrease in CBV (13 ± 3 %), but no significant decrease in CBF except in the contra-lateral temporal region (28 %).

This thesis also presents the validation of a method to measure regional CBF using contrast enhanced CT through the application of the Central Volume Principle and the technique of deconvolution. Regional CT CBF measurements were compared to those simultaneously obtained with the 'gold' standard microsphere method in rabbits under normal conditions. A strong correlation was found between rCBF values derived by the CT and microsphere methods ($r = 0.835$).

**Keywords:** cerebral blood volume, cerebral blood flow, Propofol, Isoflurane, contrast-enhanced CT, brain tumours, microspheres, two compartment model, hyperventilation.

**ACKNOWLEDGMENTS**

Over the past couple of years, I have had the opportunity to meet and work with many individuals who have been and will remain a very positive influence in my personal life and future career in the medical field. I would like to thank all of these people from The Robarts Reseach Institute, London Health Sciences Centre (University Campus), The University of Western Ontario and St. Joseph's Health Centre in London, Ontario.

Most of all, the presented MSc work and thesis would not be possible without the guidance, motivation, and support of my supervisor, Dr. Ting-Yim Lee. I would like to thank Ting for his patience and consideration for *putting up* with me during my Masters, for being a supervisor who *truly* takes the time to help his students, and for giving me the chance to participate in such interesting research. Special thanks to Dr. Brian Rutt, Dr. David Holdsworth, and Dr. Rosemary Craen for being a part of my advisory committee. Also, further thanks to Rosemary for her assistance, teachings and guidance in my research work.

Moreover, my Masters would not be complete without the help of Dr. Adrian Gelb. Thank you Dr. Gelb for your support and instruction in the anaesthesia work of this thesis. Also, I am thankful to Ms. Sarah Henderson for performing all the work needed to successfully complete the animal experiments; those late night experiments will not be forgotten. To the ladies at the CT suite of St. Josephs, thank you for your consideration and patience, especially when Emerg scans were required. Also, to Dr. Darius Nabavi, thanks for all your help with writing manuscripts and dealing with stressful situations, as well as taking the time to teach me clinically relevant information.

I would also like to thank the Physics and Medical Biophysics departments at The University of Western Ontario for providing me with a Teaching Assistant position over the past few years. Special thanks to Dr. Kanthi Kaluarachchi; your support and thoughtfulness will not be forgotten.

From a personal point of view, thanks to "The Boys" for being around when a break from my research was really in need. To the "The Girls" at Robarts, thank you for helping me out when I started my Masters. Further thanks to Laura Stevens for her assistance in the PVA phantom experiments.

Due to the clinical relevance of this research work, I have had plenty of exposure to the clinical practise of medicine. These experiences have strengthened my desire to further pursue my dream to be a physician-scientist. Moreover, words can not describe my gratitude to Dr. Rosemary Craen, Dr. Darius Nabavi and Ting for their profound support and motivation to pursue my dream; you will all remain in my memories when I look back at this chapter in my life.

Finally, to my father, mother, brother, and sister-in-law, thanks for the undying support throughout my never-ending education and to pursue my dream; your love and teachings are the pillars of my life. *"Ja vas volim puno"*. To my eternal friend, Mike, your understanding and infinite hours of dealing with me will not be forgotten; God Bless You and may our dreams come true. At last, my *"seka"* Aleksia, thanks for believing in me.

P.S. Thanks to PF, BS, and all the rest!!!

**TABLE OF CONTENTS**

## LIST OF TABLES

## LIST OF FIGURES

# 1.0 INTRODUCTION

## 1.1 INCIDENCE AND DEVELOPMENT OF BRAIN TUMOURS

Brain tumours can be divided into two groups: primary and metastatic. Primary brain tumours are those which originate within the cranium. These types of brain tumours comprise approximately 2% of all cancers in Canada and account for about 2.5% of all cancer deaths [Statistics Canada, 1998]. Moreover, primary brain tumours are responsible for most childhood cancers and show a steady rise in occurrence in adults between the ages of 50 and 70 [Johnson and Young, 1996].

Metastatic brain tumours arise from the spread of remote cancers growing outside of the central nervous system (e.g., lung, breast). By means of invasive proliferation, these cancer cells can break away from the primary site and enter nearby blood vessels. Some of these tumour cell clusters may travel to the brain where they lodge within capillaries and start to multiply locally producing metastases. The most common sources of metastatic brain tumours are lung tumours in men and breast tumours in women [Johnson and Young, 1996]. Such findings are accounted for by the fact that the nearest cluster of high flow capillaries found by the circulating breast or lung tumour cells are located within the brain. Due to the fact that lung and breast cancers account for a large proportion of adult cancers in Canada, the incidence of metastatic brain tumours significantly outnumbers primary brain tumours. In 1995, it was estimated that the total number of cancer deaths with intracranial metastases was over 25% [Johnson and Young, 1996].

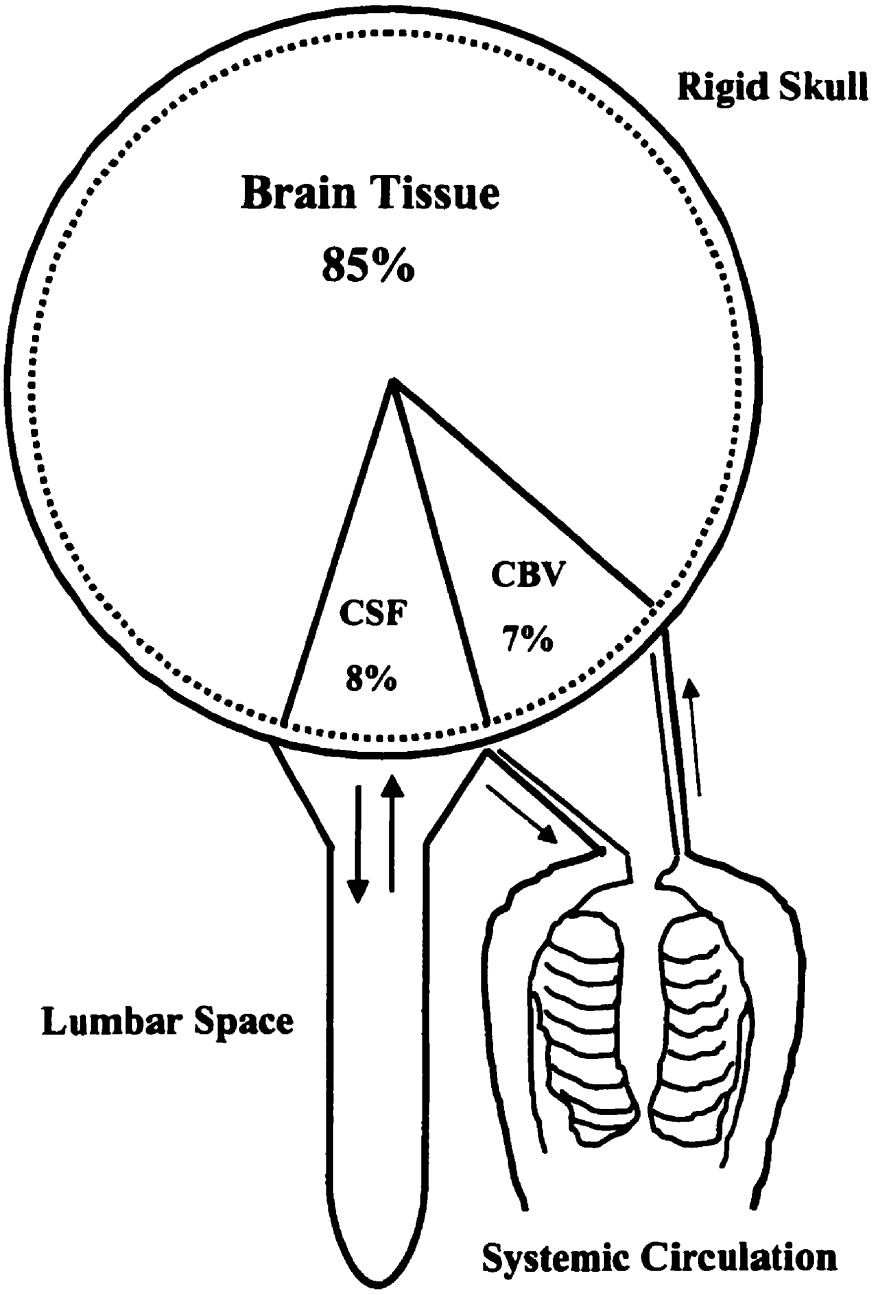


**Figure 1.1. Intracranial Components.**
The intracranial contents are housed within the rigid confines of a fixed-volume cranial vault of approximately 1400 to 1700 ml [Thapar et al., 1995].

## 1.2 IMPORTANCE OF CBV AND ICP IN BRAIN TUMOUR PATIENTS

Constant intracranial pressure (ICP) is crucial for homeostasis and therefore proper brain function. As shown in Figure 1.1, the total brain volume is comprised of three main components: tissue, cerebrospinal fluid (CSF), and cerebral blood volume (CBV). CSF is the fluid that flows within the ventricles and the sub-arachnoid space and one of its primary functions is to protect and cushion the brain and spinal cord from physical injury. CSF comprises approximately 8% of the intracranial volume. CBV is the total volume of blood within the cerebral vessels (i.e., arteries, capillaries, and veins). The arterial blood volume is controlled by the diameter of cerebral arteries and arterioles, the so-called resistance vessels which have the capacity to constrict or dilate. Venous blood volume is largely determined by the amount of blood in the sinuses. CBV accounts for only 7% of the total intracranial volume. However, it has been shown to be a major determinant of ICP [Artru, 1987]. Since the brain constituents are located within a bony, rigid skull, a volume increase in any one of these brain components must be followed by a corresponding decrease in the volume of another in order to maintain a constant ICP. When one component increases, such as tissue mass in brain tumours, without a compensatory decrease in CBV and/or CSF, ICP may rise beyond normal physiological levels (5 – 15 mmHg) [Thapar et al., 1995].

The volume of an intracranial tumour is the sum of the malignant tissue mass and the associated blood vessel density. In tumours, an increase in CBV is often seen and results from the ability of most malignant tumours to evoke extensive blood vessel formation within the mass (i.e., angiogenesis). As a tumour starts to grow, the brain compensates for the initial increase in volume by caudally displacing small amounts of

CSF into the lumbar space [Thapar et al., 1995]. Such a mechanism prevents an initial global increase in ICP. However, as shown in Figure 1.2, this volumetric compensatory mechanism has a limited capacity; upon its exhaustion, any further small increase in tumour mass and/or CBV results in a marked increase in global ICP. Raised ICP can result in the compression of vital brain tissue and arteries, and various herniation syndromes. Compression of cerebral arteries can lead to stroke, while compression of brain stem structures results in respiratory arrest. Herniation may occur through the foramen magnum which often results in death [Thapar et al., 1995].

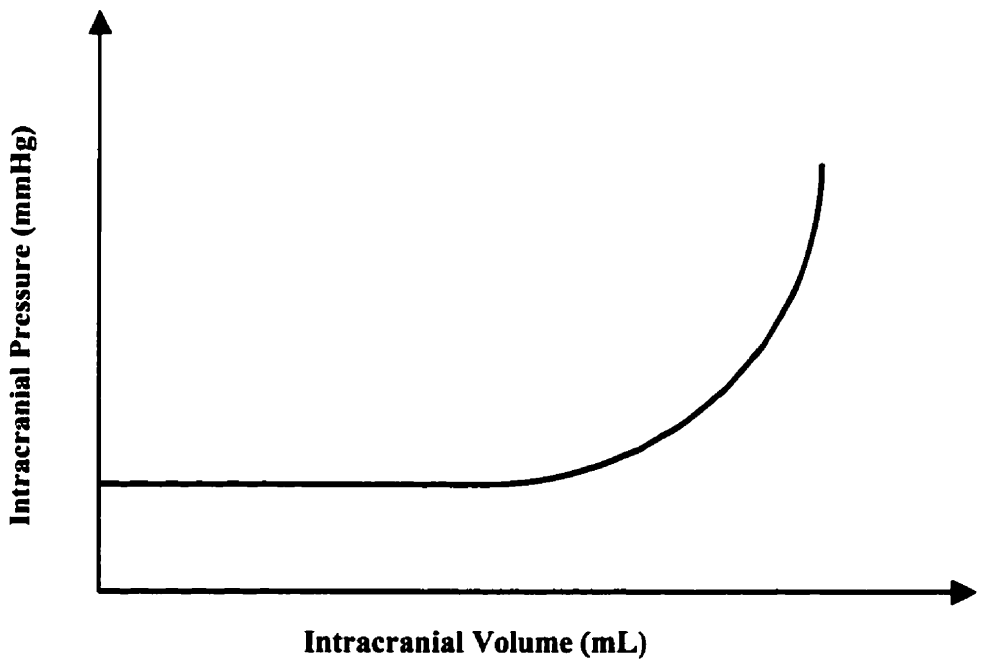


**Figure 1.2. Intracranial Pressure-Volume Dynamics.**
The brain's volumetric compensatory mechanism is represented by the plateau region that maintains a constant ICP with initial increases in volume [Thapar et al., 1995].

## 1.3 CBF AUTOREGULATION IN NORMAL AND TUMOUR CONDITIONS

The brain is absolutely dependent on continuous cerebral blood flow (CBF) for replenishment of oxygen and glucose. In humans, these metabolic requirements are met by an average CBF of 50 ml/min/100g [Harper, 1990]. Any substantial decrease below this CBF can result in ischaemia, vasogenic edema, hemorrhage, or tissue necrosis. In diseased states, decreases in CBF generally occur due to an abnormal reduction in cerebral perfusion pressure (CPP) where CPP is defined as mean arterial pressure (MAP) minus ICP. In the normal brain, a protective physiological mechanism exists that prevents brain ischemia during decreased CPP, and capillary damage during increased CPP. This physiological regulatory mechanism is termed *cerebral autoregulation.*

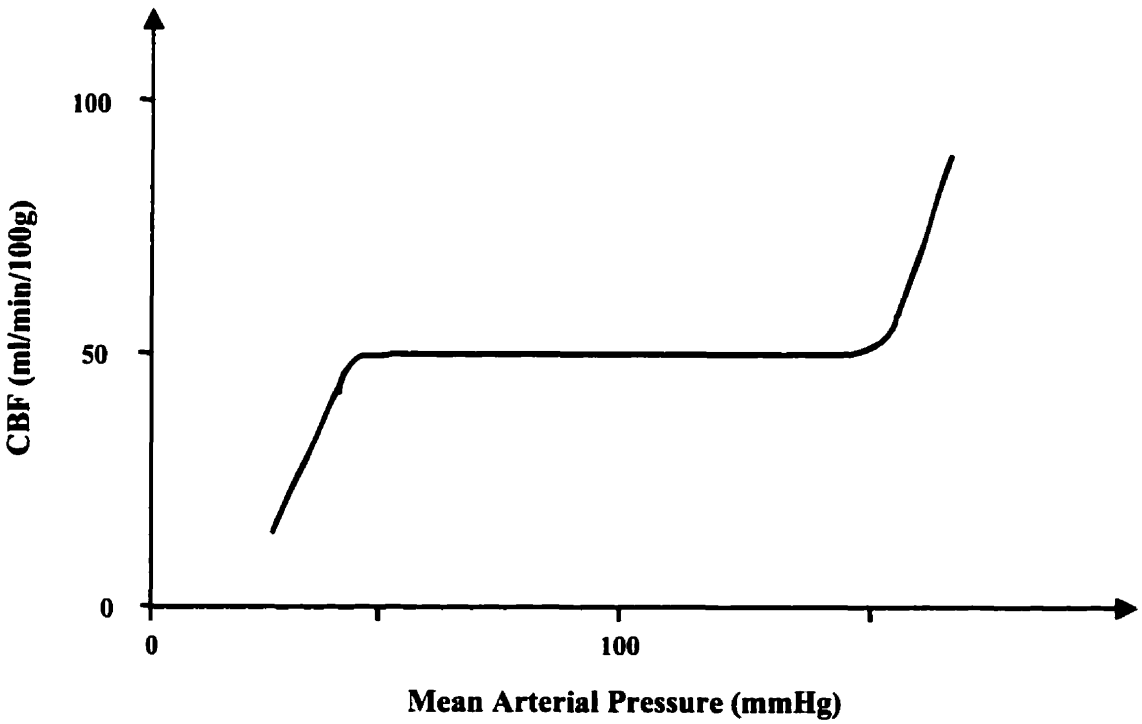


**Figure 1.3. CBF as a function of Mean Arterial Pressure.**
The plateau represents the brain's autoregulatory mechanim to maintain a constant CBF over a wide range of MAP [Harper, 1990].

Cerebral autoregulation is the intrinsic capacity of the brain to regulate CBF due to the excitable contractile process of smooth muscle that acts to constrict or dilate cerebral arterioles in response to changing arterial pressure and metabolic demands of the brain. As shown in Figure 1.3, autoregulation maintains a constant CBF despite variations in systemic MAP. In theory, without autoregulation, a decrease in MAP would decrease CPP and hence would ultimately decrease CBF to ischaemic levels. However, CBF is maintained at a normal level through the vasodilatory response of the arterioles resulting in a decreased cerebrovascular resistance (CVR), or increased CBV. In contrast, with an increase in CPP due to raised MAP, the vessels constrict, thus maintaining normal CBF by increasing CVR, hence reducing CBV. This autoregulatory mechanism is maintained only for MAPs between 50 and 150 mmHg [Harper, 1990]. Below or above these limits, normal CBF values can not be maintained due to the limited capacity of vessels to dilate or constrict. Below 50 mmHg MAP, cerebral vasodilation is at its maximum. Although CVR is maximally reduced (CBV at maximum), CPP is still very much reduced such that CBF decreases in a pressure-passive fashion resulting in ischaemia and eventually tissue cell death. Above 150 mmHg MAP, CBF also increases in a pressure-passive fashion producing cerebral hyperemia and disruption of blood-brain barrier leading to vasogenic edema or even hemorrhage which would increase ICP [Harper, 1990].

The autoregulatory response of CBF to CPP changes can be impaired or lost in most neurological diseases (acute ischemic lesions, intracranial mass lesions, and traumatic lesions) [Paulson et al., 1990]. In spite of the wide range of etiologies, the final common pathway of dysfunction is cerebral vasomotor paralysis -- the inability of cerebral vessels to respond to alterations in CPP [Paulson et al., 1990]. It is generally

believed that in cases where the CPP autoregulatory response is affected by neurological disease, the CBF regulatory response to $PaCO_2$ induced changes remains intact -- "dissociated vasoparalysis" [Paulson et al., 1990]. It would appear that autoregulation may be more susceptible to cerebral insult brought on by neurological disease than other cerebral regulatory mechanisms (e.g., $CO_2$ reactivity).

In intracranial tumours, CBF autoregulation may be affected in the focus of the lesion and in the surrounding tissue, as well as in areas remote from the mass [Palvolgyi, 1969; Endo et al., 1977]. Palvolgyi found that while autoregulation appeared to be mostly impaired in the peri-tumour region of human brain tumours, it was intact in the rest of the brain [Palvolgyi, 1969]. It has been speculated that the deranged autoregulatory response seen in the peri-tumour region may be due either to the presence of substances released by the tumour or to the fact that tumour microvessels -- lacking arterioles -- are less responsive to chemical/metabolic factors [Farrell, 1988]. In another study of regional CBF measurements in brain tumour patients, Endo found that the loss of autoregulation was observed in hyperemic sites remote from the tumour, and in most cases, peri-tumour regions also revealed signs of hyperemia [Endo et al., 1977]. Autopsy reports from this study suggest that these remote regional CBF abnormalities depended largely on the site of the tumour and were brought on by local tissue compression against rigid anatomical structures (e.g., the tentorium, or the falx) [Endo et al., 1977]. Besides Palvolgyi's and Endo's studies, there is very little data regarding cerebral autoregulation in the presence of a brain tumour. These studies, however, do suggest that regional CBF is grossly irregular in brain tumour patients, and loss or impairment of autoregulatory

mechanisms may occur locally and, at times, diffusely throughout both cerebral hemispheres.

## 1.4 AUTOREGULATORY EFFECTS OF $PaCO_2$ ON CBV AND CBF IN NORMAL AND TUMOUR CONDITIONS

CBV, and consequently CBF, is directly proportional to the cross-sectional radius of cerebral blood vessels to the fourth power [Miller and Bell, 1987]. In turn, the calibre of cerebral arteries and arterioles is regulated by a variety of chemical/metabolic, neurogenic, and myogenic influences. The chemical/metabolic factors (e.g., arterial $PaCO_2$, and extracellular fluid concentration of K+ ion) are believed to be the most important regulators of CBV and CBF [Young and Ornstein, 1994].

Arterial carbon dioxide is one of the most effective chemical mediators of CBV and CBF [Paulson et al., 1990]. The mechanism of action of carbon dioxide on arteries and arterioles is believed to be through changes in the hydrogen ion concentration of the extracellular fluid (ECF) surrounding these vessels -- vasodilation resulting from an acidic ECF, and vasoconstriction from an alkaline ECF. Therefore, during hyperventilation, the carbon dioxide concentration decreases in arteries and in the ECF (i.e., hypocapnia), thus resulting in an increased pH level. Whereas during hypoventilation, the arterial and ECF $CO_2$ levels (i.e., hypercapnia) increase, thus decreasing pH. As shown by Grubb in healthy primates, changes in CBV and CBF are approximately linear to changes in $PaCO_2$ in the range 20-70 mmHg [Grubb et al., 1974]. However, the change in CBV is substantially less than CBF for each mmHg change. For each 1 mmHg change in $PaCO_2$, CBV changes by 0.041ml/100gm, and CBF changes by 1.8 ml/min/100gm [Grubb et al., 1974].

CBF reactivity to arterial carbon dioxide changes has been investigated in brain tumour patients [Palvolgyi, 1969]. In this study, $CO_2$ reactivity was investigated in the ipsi-lateral non-tumour tissue and the pathological mass. Hypercapnia induced an increase in CBF in the whole hemisphere except in the tumour region. In the tumour, a paradoxical flow decrease was observed in most patients during hypercapnia; this phenomenon is known as *intracerebral steal.* The latter refers to the decreased flow in the pathological area caused by the physiological vasodilatory response in surrounding normal tissue when hypercapnia is induced; and conversely, decreased flow in normal tissue, but an unexpected increase in the tumour during hypocapnia. This study provides important insight into the $CO_2$ reactivity of CBF in brain tumour patients; however, data on the $CO_2$ reactivity of CBV in brain tumours is not available.

Grubb's and Palvolgyi's studies have provided useful insight on CBV and/or CBF reactivity to changing $CO_2$ levels in normal and pathological conditions. However, such effects of $PaCO_2$ on CBV and CBF cannot be accurately extrapolated to conditions where anaesthetic agents are used in normal patients or patients with cerebrovascular disease (e.g., brain tumours) due to the vasoactive effects of anaesthetics.

## 1.5 CEREBROVASCULAR EFFECTS OF ISOFLURANE AND PROPOFOL ANAESTHESIA

Anaesthetic agents are vasoactive in that they can either constrict or dilate blood vessels. Such vasoreactivity can result in potentially deleterious cerebrovascular and cerebral metabolic effects in brain tumour patients undergoing neuroanaesthesia. Knowledge about the hemodynamic effects of a given agent on normal, as well as on

diseased tissue, is necessary for the effective management of patients undergoing neuroanaesthesia. Inhalation anaesthetics (e.g., Halothane, Isoflurane) generally increase CBV through the vasodilation of cerebral vessels, and hence increase CBF. In contrast, intravenous anaesthetics (e.g., Thiopental, Propofol) decrease CBV and CBF by constricting blood vessels. Thus, the ideal anaesthetic agent for a patient with raised ICP undergoing surgical resection of a brain tumour is one which reduces ICP (through decreased CBV), and still maintains cerebral autoregulation and cerebrovascular carbon dioxide reactivity.

In our studies, we employ two commonly used neuroanaesthetics: Isoflurane and Propofol. The vasodilatory effects of Isoflurane are concentration-dependent. Up to 1 MAC (minimum alveolar concentration) Isoflurane does not increase CBF in rabbits or humans, but thereafter CBF increases [Scheller et al., 1987; Eger, 1985]. Thus, Isoflurane concentrations above 1 MAC are cautiously used in patients with raised ICP since an increase in CBF is known to increase CBV, hence further increase ICP. Currently, Isoflurane is used in conjunction with hyperventilation with the belief that decreasing $PaCO_2$ below 30 mmHg negates the Isoflurane-induced increase in CBF and presumably CBV. However, various studies in rabbits have shown that for the same degree of hyperventilation with Isoflurane, there is a differential reduction in CBF (52%) [Scheller et al., 1986] compared with CBV (25%) [Weeks et al., 1990]. In our laboratories, a differential reduction in CBF (26%) and CBV (14%) was also found in normal rabbits upon hyperventilation during Isoflurane anaesthesia [Howard, 1996].

Propofol is an intravenous anaesthetic agent that induces a rapid onset and offset of anaesthesia compared to most commonly used volatile and intravenous anaesthetics.

*In-vitro*, Propofol has been shown to vasodilate cerebral arteries [Gelb et al., 1996]. However, *in-vivo*, induction of Propofol has shown to reduce both CBF by 51 % and cerebral oxygen consumption ($CMRO_2$) by 36 % [Stephan et al., 1987]. This *in-vivo* response can be explained by the coupling between CBF and $CMRO_2$ that overrides Propofol's intrinsic vasodilatory effects as shown *in-vitro*. The CBF response to hyperventilation during Propofol anaesthesia was examined in humans and revealed a smaller reduction in CBF than in awake humans (i.e., voluntary hyperventilation) [Craen et al., 1992]. Due to the fact that cerebral vessels have a limited capacity to vasoscontrict, this reduced responsiveness to hypocapnia is believed to reflect the already constricted state of the vessels brought on by induction of Propofol. However, this same study also revealed that upon hyperventilation, CBF decreased to levels approaching that of the cerebral ischaemic threshold. Recently, the effects of induced hypocapnia during Propofol anaesthesia on CBF and CBV were investigated in normal rabbits [Howard, 1996]. This study showed that, unlike Isoflurane, Propofol caused a small reduction in CBF (14%) and no significant change in CBV upon reducing $PaCO_2$ below 30 mmHg. These results suggest that the combination of normocapnia ($PaCO_2$ of 40 mmHg) and Propofol anaesthesia already produces a maximal constriction of blood vessels which have very little remaining capacity to constrict any further upon hyperventilation. Such findings have important clinical implications because if hyperventilation produces no further reduction in CBV during Propofol anaesthesia, there may be no benefit inducing hypocapnia during Propfol anaesthesia in patients with raised ICP. Moreover, the accompanying low CBF may put the patient at risk of cerebral ischaemic injury.

Hyperventilation is commonly employed during neuroanaesthesia for brain tumour patients in the belief that CBV and therefore ICP will be reduced. While there is some information on the effect of hyperventilation on regional CBV and CBF in brain tumours, there is no available information on the combined effects of anaesthetics and hyperventilation. Our study will be the first to attempt to quantify the effects of hypocapnia with two commonly used neuroanaesthetics (Propofol and Isoflurane) on regional CBV and CBF in brain tumours.

## 1.6 RATIONALE OF *IN-VIVO* CBV AND CBF MEASUREMENTS USING COMPUTED TOMOGRAPHY

An ideal method to measure CBV and CBF depends on the clinical availability of equipment, cost, subject (human versus animal), the invasiveness of the procedure, and the ability to perform repeated *in-vivo* measurements in the same subject. From a clinical perspective, an especially important consideration is the ability of the technique to provide adequate anatomic spatial resolution so that the absolute regional measurements of CBV and CBF can be correlated with the cerebral structures of interest.

Currently, Positron Emission Tomography (PET) is the gold standard method for *in-vivo* CBV and CBF measurements [Tyrrell, 1990]. It has been used to measure both CBV and CBF in patients with various cerebrovascular diseases (e.g., stroke, intracranial tumours), cerebral degenerative disease (e.g., Alzheimer's), and epilepsy [Tyrrell, 1990]. However, due to the high capital and operating costs associated with PET, it is not clinically available in most health care institutions in the U.S. and Canada. With the general availability of Computed Tomography (CT) scanners in most hospitals across North America, and the potential advantages of measuring CBV and CBF in the

diagnosis, prognosis, and clinical management of cerebrovascular disease, we developed a method to measure these cerebral hemodynamic parameters using CT.

Besides its clinical availability, there are three main advantages of using CT over PET scanners in studying cerebral perfusion parameters. First, CT scanners have better spatial resolution than PET (less then 1mm compared to 3-4 mm). Such spatial resolution allows very small critical structures to be imaged so that the functional information obtained can be correlated directly to anatomy without the need of image registration. Second, since the detected signal of the CT scanner is directly proportional to the attenuation properties of the tissue, its ability to provide accurate measurements is unsurpassed by PET and other imaging modalities (the PET signal is affected by tissue attenuation and random coincidence). Finally, in regards to image acquisition, CT has better temporal resolution than PET. With the advent of slip-ring CT scanners, cine scanning -- continuous acquisition of images at the rate of one every second or less -- is possible. Such fast (cine) CT imaging allows one to accurately follow the passage of a bolus of contrast material through the brain.

Stable xenon-enhanced computed tomography (Xe/CT) has also been used successfully to measure CBF in brain trauma injury patients and has been validated in baboons with radio-labeled microspheres [Dewitt et al., 1989]. However, due to the high costs and inherent vasoconstriction effects of xenon gas [Goldman, 1993], Xe/CT has not found much support in the clinical environment.

We developed and implemented a contrast enhanced CT scanning technique to measure regional CBF, CBV, and mean transit time (MTT) -- the average time taken by blood to traverse a capillary network -- in the same physiological units as PET and

Xe/CT [Cenic et al., 1997]. In comparison to Xe/CT, the iodinated contrast agent used in our studies is an inert compound that does not induce vasoactive effects. Therefore, our contrast enhanced CT method allows one to accurately evaluate the effects of various neuroanaesthesia procedures and therapeutic drug regimens on cerebral hemodynamics.

## 1.7 RESEARCH GOALS

The goals of our research were:

(1) to study the effect of hyperventilation on regional CBV and CBF during Propofol or Isoflurane anaesthesia in a rabbit brain tumour model. Regional CBV was measured *in-vivo* through analysis of data collected by contrast enhanced CT scanning with a two compartment tracer kinetic model. Regional CBF measurements were simultaneously acquired using the *ex-vivo* microsphere technique.

(2) to validate an *in-vivo* CT method of measuring regional CBF in a normal rabbit brain model against the 'gold' standard technique of microspheres. As well, to develop and apply a method to correct for Partial Volume Averaging when imaging small arteries (e.g., cerebral, ear, radial) during contrast enhanced CT studies of CBV and CBF.

## 1.8 THESIS OUTLINE

### *1.8.1 Anaesthesia and Hyperventilation Effects on CBV and CBF in Brain Tumours*

Chapter 2 presents our study investigating the combined effects of hyperventilation and anaesthesia on regional CBV and CBF in a rabbit brain tumour model with two commonly-used neuroanaesthetic agents: Propofol and Isoflurane. This study implemented a contrast enhanced, *in-vivo* CT method to measure regional CBV while regional CBF was simultaneously measured using the well-established *ex-vivo* method of microspheres. A brief description of the non-equilibrium, two compartment tracer kinetics model used to acquire CBV measurements in normal and pathological tissue is presented. This model and associated CT scanning protocol were previously developed and implemented by Yeung [1994], Howard [1996], and Stevens [1997]. Improvements in this CT scanning method were also developed (e.g., simultaneous radial artery scanning) in order to increase the accuracy and simplicity of this technique. This chapter is based in part on a paper entitled "Dynamic Contrast Enhanced X-ray CT Measurements of Cerebral Blood Volume in a Rabbit Tumour Model" which was published in SPIE's Medical Imaging '98 Proceedings [Cenic et al., 1998].

### *1.8.2 Validation Study of a Novel In-Vivo CT-CBF Method*

Chapter 3 presents a new CT method to measure CBF *in-vivo*. The theoretical stochastic approach adopted in this CBF measurement technique is presented in detail in this chapter. To validate this new method, CBF measurements were obtained simultaneously using both the contrast enhanced CT method and the 'gold' standard *ex-vivo* method of microspheres in normal rabbits. The results of this validation study are

presented by correlating regional CT CBF measurements with regional microsphere CBF measurements. This chapter also discusses a method to correct for Partial Volume Averaging when measuring contrast enhancement in small blood vessels (e.g., arteries). A phantom consisting of tubes of various sizes was developed for this correction procedure. The experimental CT imaging protocol and analysis method to acquire a calibration curve with the phantom is presented. Moreover, a description of our technique to measure the inner diameter of an imaged vessel, and hence the appropriate Partial Volume Scaling Factor for the observed contrast enhancement, is discussed. This chapter is based on a paper entitled "Dynamic CT Measurements of Cerebral Blood Flow: A Validation Study" which was submitted to AJNR: American Journal of Neuroradiology" [Cenic et al., June 1998].

### *1.8.3 Thesis Summary & Future Work*

Section 1 of Chapter 4 provides a summary of important results from Chapters 2 and 3. Section 2 presents modifications required in our CT CBF analysis method for the accurate measurement of CBV and CBF in pathological tissues with finite capillary permeability (e.g., tumour). Future experimental work will entail first validating this modified CT CBF method in a rabbit brain tumour model against the 'gold' standard microsphere method, and then applying this method to measure regional CBV and CBF in brain tumour patient studies.

# 2.0 ANAESTHESIA AND HYPERVENTILATION EFFECTS ON CBV AND CBF IN BRAIN TUMOURS

## 2.1 INTRODUCTION

Hyperventilation is a common adjunct in neuroanaesthesia for patients with intracranial mass lesions. Upon hyperventilating patients with brain tumours during neuroanaesthesia, clinicians readily observe signs of a decrease in raised intracranial pressure (ICP), such as decreased papilledema [Craen, 1998]. However, there is no experimental evidence to suggest that this decrease in ICP following induced hypocapnia is associated with a similar decrease in cerebral blood volume (CBV). Also, even though various anaesthetics are known to have different vasoactive effects on the cerebrovasculature, there is very little data to help clinicians make a rational choice of anaesthetic agent in the effective management of patients with raised ICP. In such patients, the ideal anaesthetic agent should decrease CBV significantly -- hence ICP -- while maintaining cerebral blood flow (CBF) above ischemic thresholds. The purpose of our study was to investigate whether the normal CBV and CBF responses to hyperventilation are maintained in a rabbit tumour model during two commonly used neuroanaesthetics: Isoflurane and Propofol.

Using a two compartment model to characterize the kinetics of X-ray contrast agent in the brain, we developed a non-equilibrium CT method to estimate CBV both in normal and pathological tissue [Yeung et al., 1994]. Previous investigators [Penn et al., 1975; Zilka et al., 1976] have measured CBV in normal brains with an intact blood-brain barrier (BBB). However, in cases where the BBB breaks down (e.g., tumour), such methods would overestimate CBV since the distribution volume of the contrast agent would be a sum of the intravascular (IVS) and extravascular (EVS) spaces. In contrast,

our two compartment model explicitly accounts for any leakage of contrast agent across the BBB and hence is able to give accurate CBV measurements even in pathological tissue. In the anaesthesia studies, regional CBF measurements were simultaneously made with the well-established technique of microspheres.

## 2.2 X-RAY CONTRAST AGENT KINETICS MODEL

Our CT CBV measurement technique uses a two compartment model of the brain to describe the distribution of X-ray contrast agent in IVS and EVS. Using our two-compartment method of analysis, regional CBV values were determined from the measured CT contrast enhancement curves of arterial blood and brain tissue as shown in Figure 2.1.

The contrast agent we used in this study was iopamidol (Isovue 300, Squibb Diagnostics). It is a non-ionic and biologically inert hydrophilic molecule [Morris and Fischer, 1986] that can passively diffuse across the BBB when the latter is compromised in pathological conditions. Since iopamidol does not permeate the bi-lipid layer of cell membranes, it can only distribute in the IVS and the extravascular, extra-cellular space (EES) of tissue. Thus, in the case of normal brain tissue, iopamidol remains entirely intravascular, but in diseased brain, its distribution volume is comprised of both the IVS and the EES.

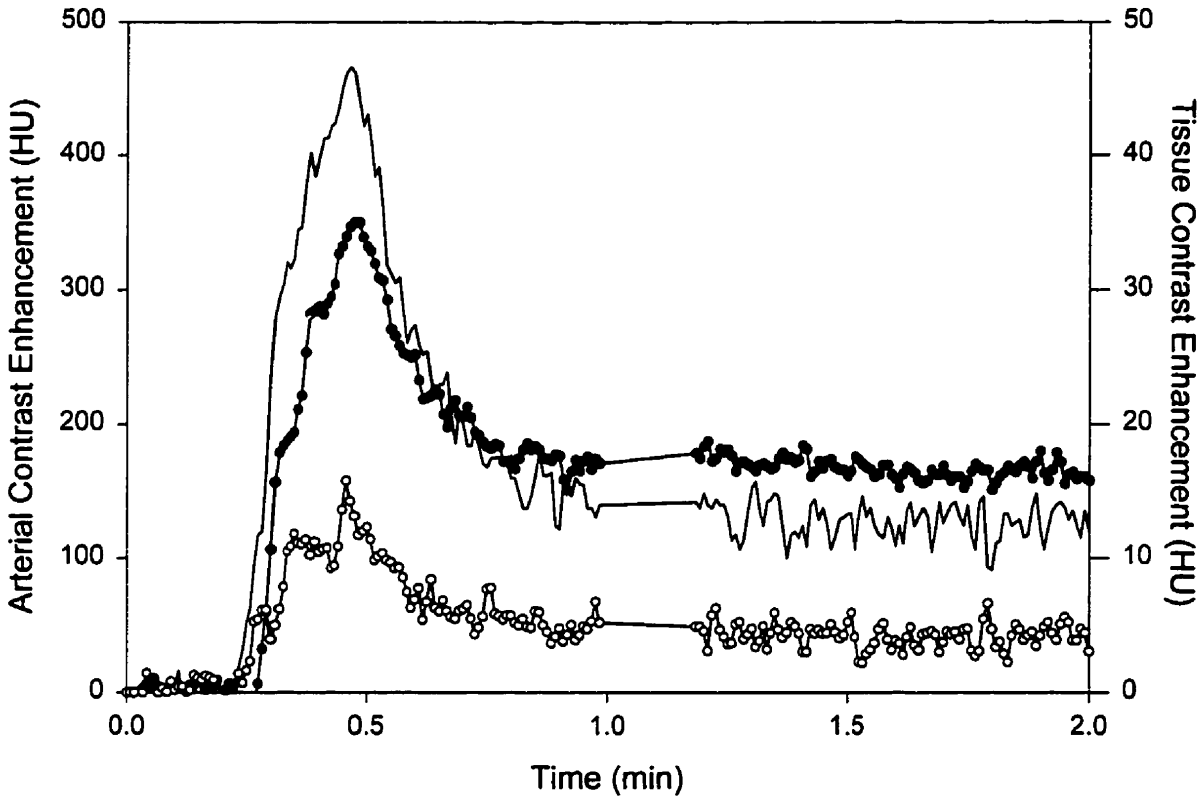


**Figure 2.1. Dynamic CT Contrast Enhancement Curves in a Brain Tumour Rabbit.**

The arterial curve (-) was measured in a radial artery. The tumour tissue (•) curve reveals a larger peak enhancement than in the contra-lateral normal tissue curve (o). The 5 sec delay between the two cine CT scanning groups is shown by the missing data points at the 1 min time interval.

In order to describe the kinetic behaviour of contrast in the brain, a special case of the two compartment model [Patlak et al., 1983; Patlak and Blasberg, 1985; Yeung et al., 1994] was used as shown in Figure 2.2. In this model, the IVS compartment represents the CBV with the BBB separating it from the EES. The EES is also assumed to be a compartment such that diffusion of contrast within it is not considered in the model. The following model parameters were used in the subsequent derivation that characterizes the distribution of contrast agent in the brain:

| | |
|---|---|
| $C_a(t)$ | contrast concentration in the IVS at time 't' (mmol/ml); this is measured by the arterial blood enhancement curve in Houndsfield units [see Section 2.4.2] |
| $C_e(t)$ | contrast concentration in the EES at time 't' (mmol/ml) |
| $Q(t)$ | mass of contrast in the brain tissue (mmol/g); this is measured by the tissue enhancement curve in Houndsfield units [see Section 2.4.1] |
| CBV | distribution volume of contrast in the IVS (ml/g) |
| $V_e$ | distribution volume of contrast in the EES (ml/g) |
| K | unidirectional transfer 'rate' constant of contrast from IVS to EES (ml/min/g) |
| k | backflux rate constant from EES to IVS ($min^{-1}$) |

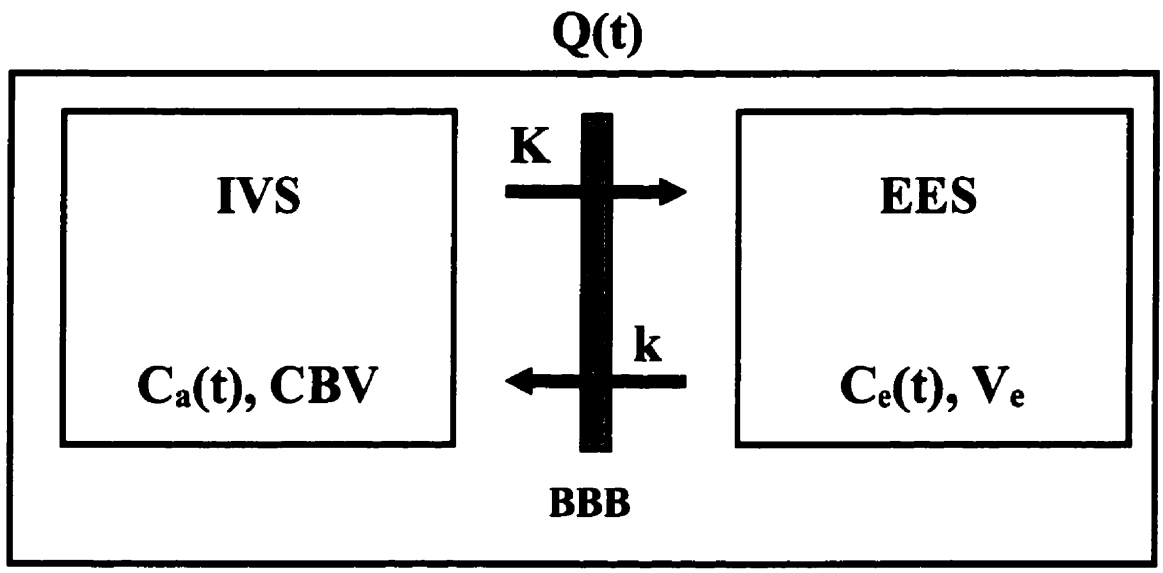


**Figure 2.2. Two Compartment Model Describing the Distribution of X-ray Contrast Material in the Brain.**
In normal tissue, the contrast agent distributes only in the intravascular space (IVS). In tumour tissue, the measured Q(t) or enhancement results from the contrast in both the IVS and the extravascular, extracellular space (EES).

The mechanism of exchange of contrast between the two compartments is assumed to be passive diffusion. From the Law of Conservation of Mass, the change in the mass of contrast in the EES ($V_eC_e(t)$) is given by:

$$\frac{d[V_eC_e(t)]}{dt} = -K[C_e(t) - C_a(t)] \qquad (2.1)$$

K is the unidirectional transfer 'rate' constant of contrast from blood (IVS) into the EES and is related to a property of the capillary endothelium, PS, by [Fenstermacher et al.,1981]:

$$K = CBF \times \left\{1 - \exp\left[\frac{-PS}{CBF}\right]\right\} \qquad (2.2)$$

where P is the permeability of the capillary endothelium (ml/min/cm$^2$) and S is the capillary surface area (cm$^2$); CBF is the regional cerebral blood flow (ml/min) per gram of tissue. In brain tumour regions, generally CBF >> PS; hence, PS can be approximated by K [Blasberg et al., 1983]. Letting $k = K/V_e$, Equation 2.1 becomes:

$$\frac{d[C_e(t)]}{dt} = kC_a(t) - kC_e(t) \qquad (2.3)$$

With initial conditions of $C_e(t) = 0$ at $t = 0$, the solution of Equation 2.3 gives:

$$C_e(t) = k\int_0^t C_a(u)\exp\{-k(t-u)\}du \qquad (2.4)$$

Due to the limiting spatial resolution of the CT scanner (10 lp/cm), $C_e(t)$ can not be directly measured. However, the CT scanner does measure the mass of contrast in brain tissue and concentration of contrast in an artery. Since Q(t) is comprised of both the IVS and EES, thus:

$$Q(t) = C_e(t)V_e + C_a(t)CBV \qquad (2.5)$$

Substituting Equation 2.4 into Equation 2.5, we obtain the following model equation for Q(t):

$$Q(t) = K\int_0^t C_a(u)\exp\{-k(t-u)\}du + C_a(t)CBV \qquad (2.6)$$

With multiple measurements of Q(t) and $C_a(t)$ following a bolus intravenous injection of contrast agent (Isovue 300), the model parameters (CBV, K, k) can be calculated using non-linear regression methods. A constrained quasi-Newton algorithm [Gill and Murray, 1974; 1976] from the Fortran NAG Library (Downers Grove, IL) was used for the regression analysis. Since negative values of CBV, K, and k have no physiological significance, the lower limits of these model parameters were set to zero.

## 2.3 EXPERIMENTAL METHODS

### *2.3.1 Brain Tumour Model*

The VX2 carcinoma tumour was selected because it has characteristics similar to human metastatic brain tumours [Carson et al., 1982]. Also, the VX2 carcinoma tumour model has the advantages of a high rate of successful implantation, a short induction time, good reproducibility and stable histology [Zagzag et al., 1988]. The following procedure was followed in the implantation of brain tumours in rabbits. First, VX2 carcinoma cells were injected into the hind leg of a host rabbit and allowed to grow to about 3-4 cm in diameter. The host rabbit was then sacrificed and the tumour cells from its hind leg were harvested and injected into the brain of a 3 kg male New Zealand White rabbit. To obtain a standard sized tumour in a selected region of the brain, a measured number of cells (approximately $5 \times 10^5$ cells) were injected into the right parietal lobe (2-3 mm below the dura mater) through a small burr hole in the cranium. The tumour was then allowed to grow for at least six days. From day six onwards, a standard contrast enhanced CT scan of the brain was performed every other day to determine the size of the tumour. When the tumour reached approximately 0.4 cm in diameter, the anaesthesia study was performed on the following day using the protocol described below.

### *2.3.2 CT Scanning Protocol*

The CT imaging protocol involved three steps: the scout scan, the tumour localization coronal scans, and the cine (i.e., continuous scanning without interscan delay) study scans. Firstly, the anaesthetized animal was placed in the prone position on

the scanner's couch with its head and forelimbs secured in a conventional CT head holder. A lateral scout scan was then performed with the following X-ray tube parameters: 80 kVp and 40 mA. Secondly, from this lateral scout image, non-enhanced coronal scans were prescribed such that coronal images of the head were imaged at 3 mm spacing intervals with the following technical parameters: 80 kVp, 80 mA, 512 × 512 matrix size, 10 cm field of view, and 3 mm slice thickness. From these non-enhanced coronal scans, the brain tumour was localized. Upon intravenous injection of 1 ml of iopamidol, 1 mm spacing coronal scans of the same (3 mm) thickness were then performed in order to locate the coronal section with the largest tumour cross-section; this section was then chosen as the study slice for the two sequential dynamic CT studies.

Finally, with the brain tumour slice localized, contrast enhanced cine CT scans were performed (i.e., the chosen slice was repeatedly and continuously scanned without any time delay between scans). The cine imaging parameters were as follows: 80 kVp, 80 mA, 512 matrix size, 10 cm field of view, 3 mm slice thickness, and one second per scan. In the reconstruction of CT images, a *detailed algorithm* -- using a back-projection filter with a cut-off frequency of 10 line pairs per cm -- was employed. Cine scanning was initiated five seconds before a bolus of Omnipaque 300 contrast (1.5 ml per kg mass) was intravenously injected using an automated injector (Medrad Injector, Medrad, PA) with an infusion rate of 0.3 ml per second. This delay in contrast injection allowed for the acquisition of non-enhanced, baseline images (i.e., background data for image analysis). Cine scanning was maintained during the bolus injection of contrast agent and continued for a total of two minutes with a five second delay between the first and second cine group (60 scans per cine group).

### *2.3.3 Animal Protocol*

Twenty-two New Zealand White rabbits were used in these experiments which were approved by the Animal Ethics Committee at the University of Western Ontario (London, Ontario, Canada). Each rabbit (with implanted brain tumour) was surgically prepared as follows for the anaesthesia studies: mask induction of anaesthesia with halothane, an ear vein cannulated for drug administration, and a tracheotomy for mechanical ventilation. Vecuronium (muscle relaxant) was administered via the cannulated ear vein, and then the rabbit was mechanically ventilated to an arterial carbon dioxide tension ($PaCO_2$) of normocapnia (approximately 40 mmHg) with a mixture of air and oxygen. Both femoral arteries were then catheterized to allow arterial blood sampling, hematocrit (Hct) and blood gas determination (i.e., $PaCO_2$ and $PaO_2$), and the continuous monitoring of mean arterial pressure (MAP). Both femoral veins were also catheterized for fluid and drug administration if required (e.g., phenylephrine for maintenance of MAP between 75 to 85 mmHg), as well as for the measurement of central venous pressure (CVP). Halothane anaesthesia was ceased and Isoflurane (or Propofol) was used for the remainder of the study. A thoracotomy was then performed with the insertion of a catheter into the left atrial appendage. This atrial catheter permitted the injection of fluorescent (or radioactive) microspheres directly into the left atrium for the *ex-vivo* measurement of CBF. Finally, an intraventricular catheter was placed into the ventricle of the left hemisphere to monitor ICP over the duration of the experiment.

With the surgical procedures completed, the rabbit was transported to the CT scanner suite. MAP and CVP were continuously monitored, and rectal temperature was maintained at approximately 38.5 degrees Celsius with a heating pad and heat lamp. Hct

was also measured every 30 minutes to ensure that the blood volume was not rapidly decreasing due to withdrawal of blood samples for blood gas determination and microsphere-CBF measurements. Since arterial carbon dioxide measurements were not made during the CT scanning time period, blood gas measurements were obtained before and after each study; the average value was used as the $PaCO_2$ for the CT-CBV and microsphere-CBF measurements obtained in the study. $PaCO_2$ monitoring was crucial since changes in arterial carbon dioxide tension can significantly change CBV and CBF [Grubb et al., 1974].

### *2.3.4 Ex-Vivo CBF Measurements*

Regional CBF measurements were obtained using the well-established method of microspheres [Heymann et al., 1977]. Microsphere-CBF measurements were performed during the CT scanning time interval in order to ensure identical $PaCO_2$ levels for the regional CBV and CBF measurements. For each study, microspheres labeled with a particular colour (or radioisotope) were randomly selected from a collection of possible choices and then injected into the left atrium. Using a Harvard syringe pump, 3.0 ml of blood was withdrawn from a femoral artery at a rate of 1.0 ml/min for three minutes, starting one minute prior to microsphere injection. Upon completion of the experiment, tissue samples from each cerebral hemisphere at the level of the brain tumour were obtained. Fluorescent (or gamma-ray) spectroscopy was used to determine the amount of each individual type of microsphere in the brain samples corresponding to the brain regions of interest (ROIs) of Figure 2.3. Regional CBF was then calculated for each tissue sample using the equation:

$$CBF_t = \frac{N_t \times Q}{R} \qquad (2.7)$$

where $CBF_t$ is the CBF of the brain tissue sample in ml/min/100gm, $N_t$ is the number of microspheres detected in the tissue sample normalized to 100 gm, Q is the rate of aspiration (1.0 ml/min), and R is the number of spheres detected in the aliquot of blood normalized to the total volume extracted.

### *2.3.5 Time Control and Hyperventilation Experimental Protocols*

Eleven brain tumour rabbits were used for each anaesthetic study (Isoflurane or Propofol). Three rabbits were used in the time control experiments, and eight were used for the hyperventilation experiments. In the time control experiments, repeated CBV and CBF measurements were made for two normocapnia studies ($PaCO_2 \approx 40$ mmHg) separated by at least 30 minutes. This time delay allowed the kidneys to clear X-ray contrast agent from the circulation due to the previous study, thus preventing any hyperosmotic effects on the BBB due to excessive contrast concentration in the blood in the second study. These time control experiments were performed in order to determine whether the given anaesthetic agent induced any significant changes in regional CBV and CBF measurements over time. In the hyperventilation experiments, the CBV and CBF measurements were first made at normocapnia, and then at hypocapnia ($PaCO_2 \approx 25$ mmHg) with the same time delay between studies as in the time controls.


**Figure 2.3. Contrast Enhanced Coronal CT Image of a Brain Tumour Rabbit.**

Regions of interest were drawn as shown for all brain tumour studies. The tumour and peri-tumour regions (right) reveal a greater degree of contrast enhancement than the contra-lateral hemisphere. The roughly elliptical enhanced outline in the centre of the brain is due to contrast in large blood vessels.

### *2.3.6 Statistics*

Statistical analysis was performed using the Jandel Scientific Software Package ('Sigma Plot' and 'Sigma Stat'). Standard descriptive statistics, such as mean ± standard deviation (SD), were calculated. A *paired t-test* (two-tailed) was used to determine statistically significant changes in normally distributed data (e.g., the same anaesthetic population). In cases of non-normally distributed data, a Mann-Whitney Rank Sum Test was used. A *t-test* (two-tailed) was used to compare inter-population differences (e.g., comparison of Propofol to Isoflurane data). Statistical significance was declared at the $p < 0.05$ level.

## 2.4 CT DATA ANALYSIS

The CT images were transferred from the GE High Speed Advantage scanner to a *SUN Ultra I* workstation for analysis.

### *2.4.1 Regional Measurement of Tissue Enhancement Curve, Q(t)*

In order to measure regional CBV, ROIs in the brain were drawn in the tumour, peri-tumour, contra-lateral and left temporal normal regions (as shown in Figure 2.3) using the following procedure. First, an ROI was drawn incorporating the entire tumour -- the most enhanced area of the right parietal lobe -- as shown in Figure 2.3. This tumour ROI was then reflected into the left parietal lobe to create the contra-lateral normal ROI. The peri-tumour ROI was created by expanding the tumour ROI by five to six pixels. Finally, the left temporal normal ROI was drawn so that it would encompass most of the

tissue region inferior to the contra-lateral ROI. These tissue ROIs were drawn such that no major blood vessels were present within the regions. Q(t) for each region was then obtained by subtracting the regional mean baseline CT number in pre-contrast images from the mean CT number in sequential contrast enhanced images.

### *2.4.2 Measurement of Arterial Enhancement Curve, $C_a(t)$*

The arterial contrast concentration curve, $C_a(t)$, was determined by drawing a two pixel radius circular ROI in an artery (ear, cerebral, or radial artery). As shown in Figure 2.3, three different kinds of arteries are present in the plane of the CT image. The two enhanced vessels in the middle of the brain are the posterior communicating arteries, and the lower two enhanced vessels just superior to the optic chiasm are the internal carotid arteries [Scremin et al., 1982]. Also, in the front forelimbs, the two large blood vessels (see Figure 2.3) are the radial arteries. The artery used for determining $C_a(t)$ was the one which was most apparent in the CT image (i.e., the largest and most distinct). This was done to minimize Partial Volume Averaging (PVA) inherent while imaging small objects (e.g., arteries) with CT scanners. In most rabbit studies, $C_a(t)$ was obtained from one of the radial arteries. As discussed in the measurement of Q(t), $C_a(t)$ was also determined by subtracting the mean baseline CT number in the vessel ROI in pre-contrast scans from the mean CT number in contrast enhanced scans. The measured $C_a(t)$ was then corrected for PVA using the method discussed in Chapter 3.

## 2.5 RESULTS

### *2.5.1 Propofol Anaesthesia*

#### *2.5.1.1 Time Control Group*

A paired t-test analysis revealed no significant changes ($p >> 0.05$) in $PaCO_2$, MAP, temperature, ICP, Hct, and CVP over the duration of the experiments (i.e., between the repeated normocapnia studies). The mean values for these physiological parameters are listed in Table 2.1.

**Table 2.1. Mean Physiological Parameters (±SD) for the Propofol Time Control Experiments.**

| Study (N=3) | $PaCO_2$ (mmHg) | MAP (mmHg) | Temp. (°C) | Hct | ICP (mmHg) | CVP (mmHg) |
|---|---|---|---|---|---|---|
| Normo- | 41.7 ± 4.2 | 82.3 ± 9.3 | 38.7 ± 0.9 | 36.8 ± 2.5 | 13.7 ± 0.6 | 13.3 ± 3.1 |
| Normo- | 39.5 ± 6.1 | 79.9 ± 8.4 | 38.8 ± 0.7 | 35.3 ± 0.4 | 13.7 ± 0.6 | 13.3 ± 3.1 |

Since a 512 × 512 image matrix was used with a display field of view of 10 cm, and the area (in pixels) of each rabbit's tumour ROI was determined, the cross-sectional tumour area (in $cm^2$) was calculated for each rabbit. The mean tumour cross-sectional area for the three Propofol time control rabbits is listed in Table 2.2. The age of the tumour (i.e., days post-implantation) as well as the weight of each rabbit were recorded.

**Table 2.2. Mean Values (±SD) of Tumour Area, Rabbit Weight, and Tumour Age for the Propofol Time Control Experiments (N=3).**

| Tumour Cross-Sectional Area ($cm^2$) | Tumour Age (days post-implantation) | Rabbit Weight (kg) |
|---|---|---|
| 0.116 ± 0.041 | 10.5 ± 3.5 | 3.1 ± 0.4 |

The mean CBV and CBF values for the Propofol time control experiments are listed in Table 2.3. A paired t-test analysis revealed no significant change ($p >> 0.05$) in regional CBV and CBF measurements between the two normocapnia studies separated by a time interval of at least 30 minutes.

**Table 2.3. Mean Regional CBV and CBF Values (±SD) for the Propofol Time Control Experiments.**

| Study (N=3) | Tumour ROI | Peri-Tumour ROI | Contra-Lateral Normal ROI | Left Temporal Normal ROI |
|---|---|---|---|---|
| **CBF (ml/min/100g)** | | | | |
| *Normocapnia I* | 44 ± 13 | 74 ± 15 | 68 ± 38 | 65 ± 17 |
| *Normocapnia II* | 46 ± 17 | 57 ± 19 | 52 ± 26 | 41 ± 6 |
| **CBV (ml/100g)** | | | | |
| *Normocapnia I* | 5.50 ± 1.69 | 3.91 ± 0.91 | 1.70 ± 0.18 | 1.99 ± 0.48 |
| *Normocapnia II* | 5.69 ± 1.89 | 4.21 ± 0.75 | 1.75 ± 0.20 | 2.25 ± 0.91 |

*2.5.1.2 Hyperventilation Study Group*

A paired t-test analysis revealed no significant changes ($p >> 0.05$) in MAP, temperature, ICP, Hct, and CVP over the duration of the experiments (i.e., between normocapnia and hypocapnia studies). The mean values for these physiological parameters are listed in Table 2.4.

**Table 2.4. Mean Physiological Parameters (±SD) for the Propofol Hyperventilation Experiments.**

| Study (N=8) | PaCO2 (mmHg) | MAP (mmHg) | Temp. (°C) | Hct | ICP (mmHg) | CVP (mmHg) |
|---|---|---|---|---|---|---|
| Normo- | 40.7 ± 2.0 | 85.3 ± 10.0 | 39.2 ± 0.4 | 35.4 ± 3.5 | 12.9 ± 2.9 | 11.0 ± 0.8 |
| Hypo- | 26.5 ± 2.5 | 89.0 ± 13.6 | 39.0 ± 0.4 | 34.6 ± 3.1 | 12.9 ± 2.5 | 10.6 ± 1.3 |

The mean tumour cross-sectional area, tumour age, and rabbit weight for the eight Propofol rabbits are listed in Table 2.5.

**Table 2.5. Mean Values (±SD) of Tumour Area, Rabbit Weight, and Tumour Age for the Propofol Hyperventilation Experiments (N=8).**

| Tumour Cross-Sectional Area ($cm^2$) | Tumour Age (days post-implantation) | Rabbit Weight (kg) |
|---|---|---|
| 0.156 ± 0.067 | 11.5 ± 2.3 | 3.2 ● 0.3 |

The mean normocapnia and hypocapnia regional CBV values are shown in Figure 2.4 with their associated standard deviations. Using a paired t-test, no statistically significant decrease ($p >> 0.05$) in CBV was observed in the tumour, contra-lateral and left temporal normal ROIs upon hyperventilation. However, a statistically significant decrease ($p < 0.025$) of 10 % in CBV was observed in the peri-tumour ROI upon hyperventilation.

The mean normocapnia and hypocapnia regional CBF values are plotted in Figure 2.5 with their corresponding standard deviations. Using a paired t-test, a statistically significant decrease of 18 % ($p < 0.001$) in CBF was observed in the peri-tumour region, while no significant change ($p >> 0.05$) was detected in all other regions examined.

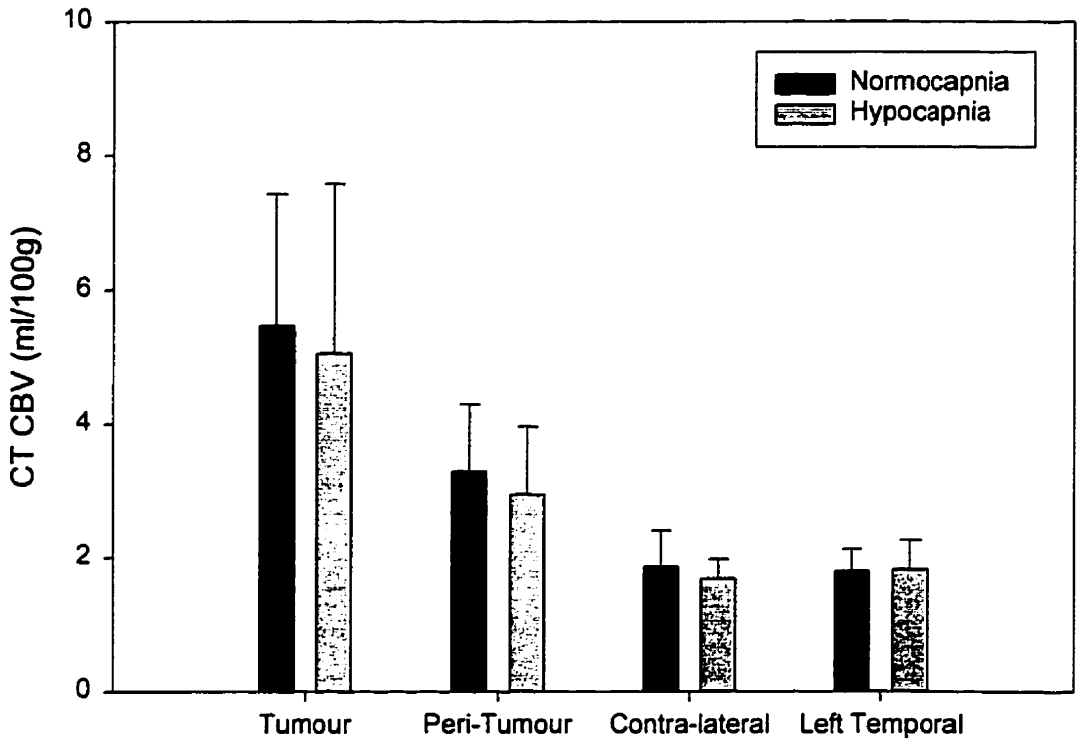


**Figure 2.4. Mean Regional CT CBV Measurements (±SD) in Brain Tumour Rabbits (N=8) at Normocapnia and Hypocapnia with *Propofol* Anaesthesia.**
A statistically significant decrease in CBV occurred in the peri-tumour region ($p < 0.025$). No significant change was revealed in the other regions upon hyperventilation ($p >> 0.05$).

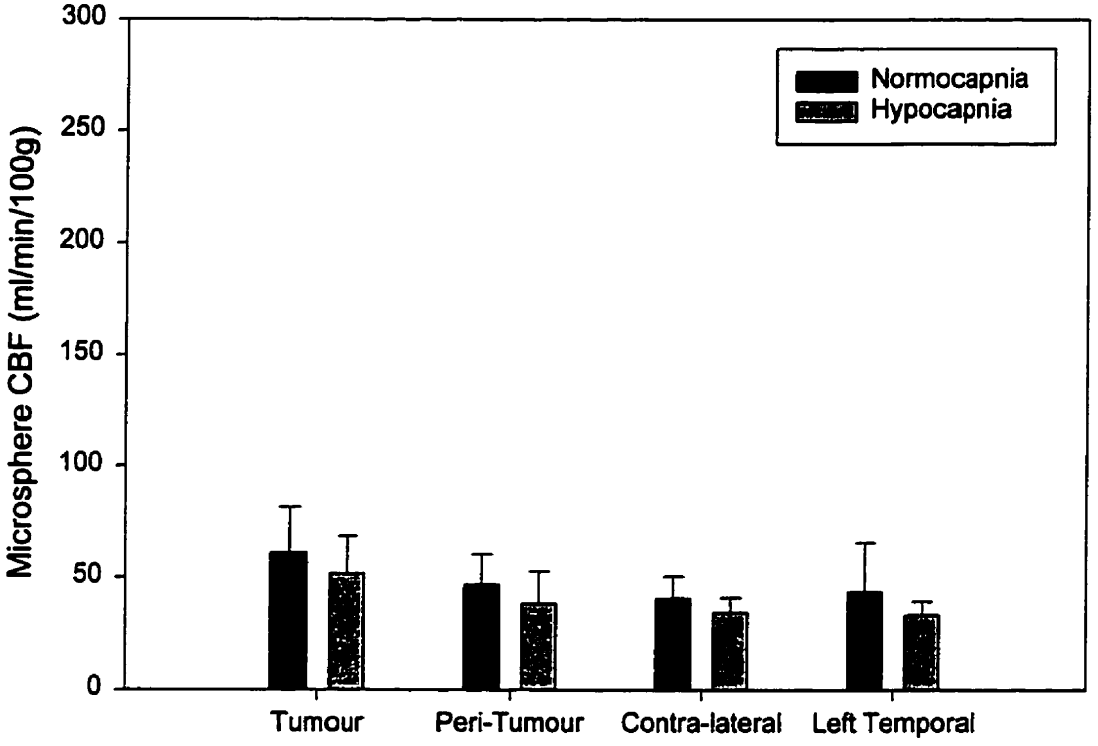


**Figure 2.5. Mean Regional Microsphere CBF Measurements (±SD) in Brain Tumour Rabbits (N=8) at Normocapnia and Hypocapnia with *Propofol* Anaesthesia.**

A statistically significant decrease in CBF occurred in the peri-tumour region ($p < 0.001$). No significant change was revealed in the other regions upon hyperventilation ($p >> 0.05$).

### *2.5.2 Isoflurane Anaesthesia*

#### *2.5.2.1 Time Control Group*

A paired t-test analysis revealed no significant changes ($p >> 0.05$) in $PaCO_2$, MAP, temperature, ICP, and Hct over the duration of the experiments (i.e., between the repeated normocapnia studies). However, a small change of 4.5 % in CVP was observed. The mean values for these physiological parameters are listed in Table 2.6.

**Table 2.6. Mean Physiological Parameters (±SD) for the Isoflurane Time Control Experiments.**

| Study (N=3) | PaCO2 (mmHg) | MAP (mmHg) | Temp. (°C) | Hct | ICP (mmHg) | CVP (mmHg) |
|---|---|---|---|---|---|---|
| Normo- | 41.0 ± 3.4 | 74.7 ± 1.5 | 39.1 ± 0.6 | 31.7 ± 2.1 | 15.0 ± 3.5 | 10.5 ± 0.7 |
| Normo- | 39.8 ± 1.6 | 73.7 ± 4.2 | 39.2 ± 0.7 | 33.8 ± 1.3 | 15.7 ± 4.0 | 11.0 ± 0.7 |

The mean tumour cross-sectional area, tumour age, and rabbit weight for the Isoflurane time control tumour rabbits are listed in Table 2.7.

**Table 2.7. Mean Values (±SD) of Tumour Area, Rabbit Weight, and Tumour Age for the Isoflurane Time Control Experiments (N=3).**

| Tumour Cross-Sectional Area ($cm^2$) | Tumour Age (days post-implantation) | Rabbit Weight (kg) |
|---|---|---|
| 0.105 ± 0.097 | 9.0 ± 3.5 | 3.2 ± 0.4 |

A paired t-test analysis revealed no significant change ($p >> 0.05$) in regional CBV and CBF measurements between the two normocapnia studies separated by at least 30 minutes. The mean values for these measurements are listed in Table 2.8.

**Table 2.8. Mean Regional CBV and CBF Values (±SD) for the Isoflurane Time Control Experiments.**

| Study (N=3) | Tumour ROI | Peri-Tumour ROI | Contra-Lateral Normal ROI | Left Temporal Normal ROI |
|---|---|---|---|---|
| **CBF (ml/min/100g)** | | | | |
| *Normocapnia I* | 119 ± 53 | 90 ± 24 | 59 ± 19 | 66 ± 28 |
| *Normocapnia II* | 119 ± 82 | 76 ± 26 | 89 ± 61 | 73 ± 35 |
| **CBV (ml/100g)** | | | | |
| *Normocapnia I* | 7.20 ± 1.62 | 3.34 ± 1.15 | 2.26 ± 0.25 | 2.69 ± 0.30 |
| *Normocapnia II* | 7.06 ± 1.61 | 3.59 ± 1.26 | 2.24 ± 0.27 | 2.88 ± 0.24 |

*2.5.1.2 Hyperventilation Study Group*

A paired t-test analysis revealed no significant changes ($p >> 0.05$) in MAP, temperature, ICP, Hct, and CVP over the duration of the experiments (i.e., between normocapnia and hypocapnia studies). The mean values for these physiological parameters are listed in Table 2.9.

**Table 2.9. Mean Physiological Parameters (±SD) for the Isoflurane Hyperventilation Experiments.**

| Study (N=8) | PaCO2 (mmHg) | MAP (mmHg) | Temp. (°C) | Hct | ICP (mmHg) | CVP (mmHg) |
|---|---|---|---|---|---|---|
| Normo- | 41.0 ± 2.6 | 77.6 ± 8.5 | 38.8 ± 0.4 | 34.4± 1.4 | 12.7 ± 3.3 | 10.5 ± 2.2 |
| Hypo- | 24.4 ± 1.2 | 76.6 ± 8.4 | 38.6 ± 0.3 | 33.4 ± 2.8 | 12.0 ± 3.4 | 10.5 ± 2.4 |

The mean tumour cross-sectional area, brain tumour age, and rabbit weight for the Isoflurane hyperventilation tumour rabbits are listed in Table 2.10.

**Table 2.10. Mean Values (±SD) of Tumour Area, Rabbit Mass, and Tumour Age for the Isoflurane Hyperventilation Experiments (N=8).**

| Tumour Cross-Sectional Area ($cm^2$) | Tumour Age (days post-implantation) | Rabbit Mass (kg) |
|---|---|---|
| 0.208 ± 0.076 | 10.0 ± 4.3 | 3.2 ± 0.3 |

The mean normocapnia and hypocapnia regional CBV values are shown in Figure 2.6 with their associated standard deviations. Using a paired t-test, a statistically significant decrease ($p < 0.02$) in CBV was observed in all the ROIs upon hyperventilation. The largest decrease in CBV of 17 % was observed in the left temporal ROI, while the smallest decrease in CBV of 11% was observed in both the tumour and contra-lateral normal ROIs. Overall, the mean global decrease in CBV from normocapnia to hypocapnia was $13 \pm 3$ % for the Isoflurane tumour rabbits.

The mean normocapnia and hypocapnia regional CBF values are plotted in Figure 2.7 with their corresponding standard deviations. Using a paired t-test, a statistically significant change of 28 % ($p < 0.01$) in CBF was observed in only the left temporal ROI, while no significant change ($p >> 0.05$) was seen in all other regions examined.

### *2.5.3 Comparison of Isoflurane and Propofol*

To compare the vasoactive effects of Propofol and Isoflurane at normocapnia, a *t-test* was used to compare regional CBV and CBF values. The mean regional CBV and CBF values for Isoflurane and Propofol are shown in Figures 2.4 to 2.7, respectively. There was a significant difference ($p < 0.05$) in all CBF and CBV values between the two anaesthetics at normocapnia. The Propofol regional CBV and CBF values were on average $30 \pm 7$ % and $54 \pm 9$ % ($\pm$ SD), respectively, lower than the Isoflurane values at normocapnia. Also, a *t-test* of regional CBV and CBF with Isoflurane at hypocapnia and Propofol at normocapnia revealed significantly larger CBV values in only the left temporal ROI (26%, $p < 0.01$), and significantly greater CBF values in the tumour and contra-lateral normal regions ($45 \pm 13$ %, $p < 0.05$) for Isoflurane.

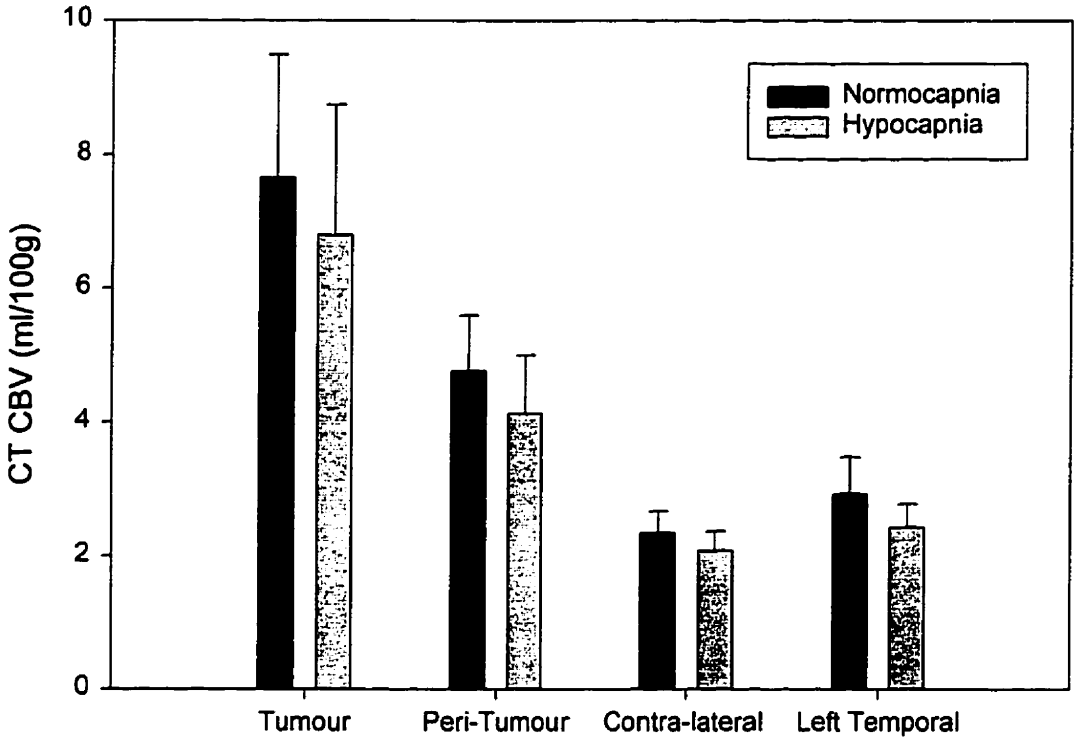


**Figure 2.6. Mean Regional CT CBV Measurements (±SD) in Brain Tumour Rabbits (N=8) at Normocapnia and Hypocapnia with *Isoflurane* Anaesthesia.** A statistically significant decrease in CBV occurred in all regions upon hyperventilation ($p < 0.02$).

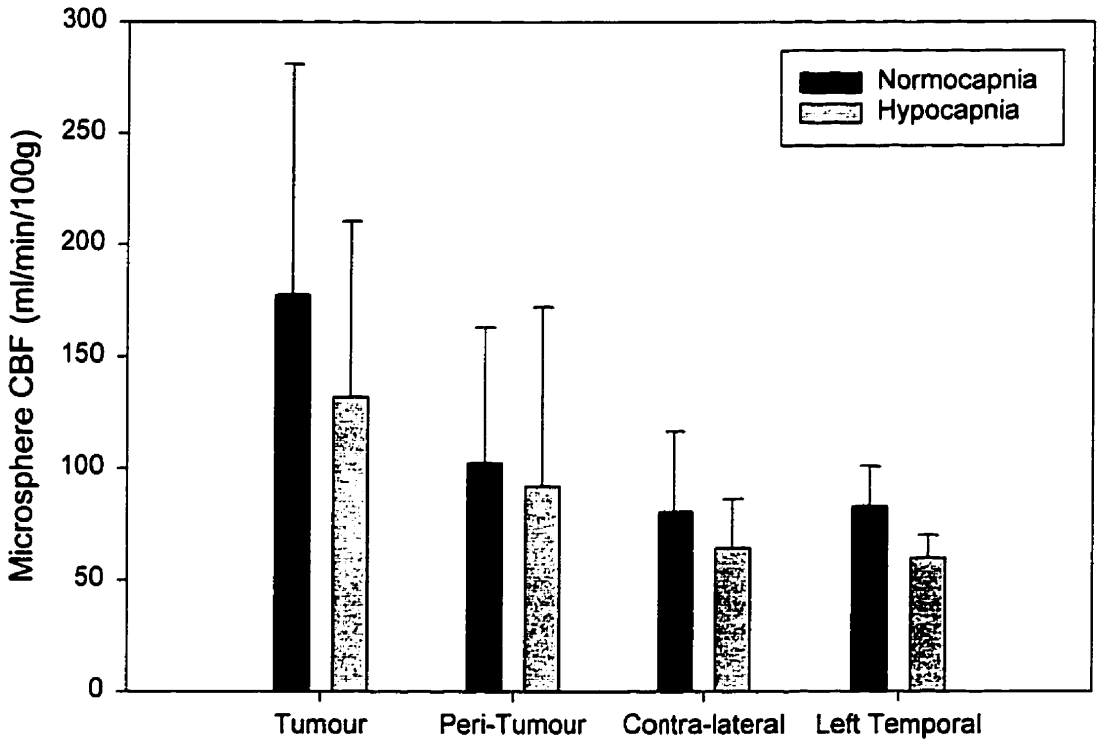


**Figure 2.7. Mean Regional Microsphere CBF Measurements (±SD) in Brain Tumour Rabbits (N=8) at Normocapnia and Hypocapnia with *Isoflurane* Anaesthesia.**

A statistically significant decrease in CBF occurred only in the left temporal region upon hyperventilation ($p < 0.01$). The other regions showed no significant change

## 2.6 DISCUSSION

### *Regional CBV Measurements in Brain Tumours*

From both anaesthesia studies, we demonstrated that the mean CBV values in tumour and peri-tumour regions are approximately 2 to 3 times greater than the mean CBV of the normal tissue regions (see Figures 2.4 and 2.6). Since CBV is directly related to vascular density, our findings support the well-established observation that capillary proliferation is a key feature of brain tumours [Zagzag et al., 1988]. The presence of tumour angiogenesis is further corroborated by the higher degree of contrast enhancement in the tumour region compared to the normal tissue of the contra-lateral hemisphere as shown in Figure 2.3. The greater enhancement in the tumour is the result of leakage of contrast across the compromised BBB in the neovasculature.

### *Propofol Anaesthesia*

There was no significant change in CBV and CBF ($p >> 0.05$) as a result of the 30 minute duration of Propofol anaesthesia in the control group. When $PaCO_2$ was altered from normocapnia to hypocapnia, there was a signifcant decrease of 10 % in CBV ($p < 0.025$) and 18 % in CBF ($p < 0.001$) in the peri-tumour ROI. However, no significant decrease in CBV and CBF ($p >> 0.05$) was observed in the tumour, contra-lateral and left temporal normal ROIs upon hyperventilation. This suggests that the CBV and CBF responses to hyperventilation are diminished in the tumour and contra-lateral normal hemisphere regions during Propofol anaesthesia while remaining intact in the periphery of the tumour. The diminished response in the tumour and normal regions may be explained by the fact that the combination of normocapnia and Propofol had already

made the cerebral arteries maximally vasoconstricted; hence, they had a limited capacity to further constrict upon hyperventilation. Such findings in both the bulk of the tumour and in the normal regions are in agreement with previous studies done in normal rabbits under Propofol anaesthesia [Howard, 1996]. In contrast, the observed decrease in both CBV and CBF in the peri-tumour region may have resulted from the fact that the feeding arterioles of the tumour (i.e., within the periphery of the tumour) are dilated more than normal [Endo et al., 1977] and hence have the capacity to further constrict upon hyperventilation. The observed differential decrease between CBV and CBF in the peri-tumour region may be partially explained by the fact that the venous system is less responsive to hyperventilation than the arterial system under Propofol anaesthesia.

Overall, these results agree with the practise of inducing hypocapnia during Propofol anaesthesia in conditions of raised ICP -- such as brain tumours -- since a significant reduction in CBV still occurs in the periphery of the tumour. However, the associated decrease in CBF to near ischemic levels must be weighed against the clinical benefit of hyperventilation during conditions of raised ICP.

***Isoflurane Anaesthesia***

There was no significant decrease in CBV and CBF ($p >> 0.05$) as a result of the duration of Isoflurane anaesthesia in the control group. When $PaCO_2$ was altered from normocapnia to hypocapnia under Isoflurane anaesthesia, an average decrease of $13 \pm 3$ % in CBV ($p < 0.025$) was observed in all the regions examined (tumour, peri-tumour, contra-lateral and left temporal normal regions). This average global decrease in CBV is in agreement with previous work done in normal rabbits under Isoflurane anaesthesia

[Howard, 1996]. However, a significant decrease of 28 % in CBF ($p < 0.01$) was observed only in the left temporal normal region which also agrees with the observed CBF response in normal Isoflurane rabbits to hyperventilation [Howard, 1996]. The other tissue regions (tumour, peri-tumour, and contra-lateral normal) revealed no significant change in CBF ($p >> 0.05$). The observed differential decrease between CBV and CBF in the left temporal normal tissue region may in part be explained by the greater response of the arterial system to vasoconstrict upon hyperventilation than the venous system.

The results of this study suggest that hyperventilation in combination with Isoflurane anaesthesia may be used when elevated ICP is a potential concern because CBV is significantly reduced while CBF is maintained at normal levels, or at least above the ischemic threshold (e.g., in the left temporal normal region).

***Comparison of Propofol and Isoflurane***

A comparison of Propofol and Isoflurane regional CBV and CBF values at normocapnia revealed significantly larger values ($p < 0.05$) for the Isoflurane study group by an average of $30 \pm 7$ % and $54 \pm 9$ %, respectively. Thus, at normocapnia, a greater degree of vasoconstriction was induced by Propofol resulting in an increased CVR, hence lower CBV and CBF values. These findings are supported by the fact that Propofol is an intravenous anaesthetic and acts as a vasoconstrictor, while Isoflurane is an inhalation anaesthetic and acts as a vasodilator (as discussed in the Introduction, Chapter 1). This observed vasoactive response by the two anaesthetics at normocapnia in the rabbit brain tumour model is in agreement with previous work done in normal rabbits under Propofol

and Isoflurane anaesthesia [Howard, 1996]. Furthermore, a comparison between regional CBV values measured at hypocapnia with Isoflurane and at normocapnia with Propofol showed that Propofol CBV values in the left temporal lobe were significantly smaller by 26 % ($p < 0.01$), while no significant difference in the other regions were observed. Since CBV is a major determinant of ICP, these results suggest that for patients with raised ICP, Propofol at normocapnia is at least as good as, if not better, than Isoflurane with hyperventilation.

## 2.7 CONCLUSIONS

To conclude, this study has demonstrated the ability of our dynamic CT method to measure the effect of $PaCO_2$ induced changes in CBV in brain tumour rabbits under Propofol or Isoflurane anaesthesia. These results will provide insight in helping anaesthetists make a more rational choice of anaesthetic agent and the use of hyperventilation in patients with raised ICP undergoing neurosurgery or ICU care.

# 3.0 DYNAMIC CT MEASUREMENTS OF REGIONAL CEREBRAL BLOOD FLOW: A VALIDATION STUDY

## 3.1 PREFACE

The brain is absolutely dependent on continuous cerebral blood flow (CBF) for replenishment of oxygen and glucose. Any interruption of CBF can result in unconsciousness (within seconds) or irreversible tissue damage (within minutes) [Harper, 1990]. The detection of changes in CBF is of utmost importance in the diagnosis and prognosis of neurological disease (e.g., tumour, stroke, Alzheimer's). Measurements of CBF are clinically important in three ways: to detect disturbances in CBF before ischaemia or irreversible brain damage occurs, to determine regions of tissue necrosis brought on by an interruption in CBF, and to monitor the effectiveness of therapeutic treatments (e.g., radiotherapy in brain tumour patients). The potential advantages of measuring CBF in the diagnosis and prognosis of cerebrovascular disease, and the general availability of CT scanners prompted us to develop a method to measure regional CBF using dynamic contrast enhanced computed tomography (CT).

This Chapter is based on a manuscript titled "Dynamic CT Measurement of Cerebral Blood Flow: A Validation Study" submitted to the AJNR: American Journal of Neuroradiology [Cenic et al., 1998]. The importance and relevance of this chapter to Chapters 1 and 2 stem from the need to develop an *in-vivo* method that simultaneously provides regional measurements of cerebral blood volume (CBV) and CBF in experimental and clinical situations. Such a method would allow investigators to avoid using highly invasive *ex-vivo* CBF measurement techniques (e.g., microspheres) in experimental settings such as the studies of Chapter 2. Furthermore, with a strong clinical demand to repeat the anaesthesia studies of Chapter 2 in patients with brain

tumours, a non-invasive *in-vivo* CT CBF method would allow such a study in humans. We undertook the study described below to assess the feasibility of our preliminary method to provide *in-vivo* CBF measurements in normal brain tissue (i.e., tissue with an intact blood-brain-barrier). Validation of this initial method in normal subjects will support future work in modifying our dynamic CT method (see Chapter 4) for the accurate measurement of CBF in pathological tissue with finite capillary permeability (e.g., tumour).

## 3.2 INTRODUCTION

Cerebrovascular disorders such as ischemic and hemorrhagic strokes constitute the third most frequent cause of death and disability in North America [Heart & Stroke Facts, 1994]. Despite considerable progress in stroke treatment, cerebrovascular disorders remain a frequent challenge in acute neurovascular management [Adams et al., 1996]. Moreover, since new therapeutic options, such as thrombolytic therapy, are expensive and are accompanied with potentially life threatening complications [Adams et al., 1996], the assessment of the risk-benefit-ratio on an individual basis is crucial for prognostic and socioeconomic reasons [Furlan and Kanoti, 1997]. Above all, the location and extent of the ischemic lesion, together with the severity of the blood flow reduction, are the main factors that predict outcome in the treatment of stroke [NINDS, 1997]. Thus, a significant clinical demand exists to assess cerebral hemodynamics in order to guide the decision between a conservative or a more aggressive form of therapy in the early stage of stroke. Several methods have been used to investigate cerebral hemodynamics in acute cerebrovascular disease [Goldman, 1993]. Positron emission

tomography (PET) is the current 'gold' standard for the *in-vivo* assessment of regional cerebral blood flow (rCBF), blood volume (rCBV), and brain metabolism [Tyrrell, 1990]. However, due to the high operational costs and low clinical availability, its application in stroke is restricted to specific scientific investigations and is not suitable for routine clinical use. Single photon emission computed tomography (SPECT) has been suggested as a tool to stratify stroke patients according to type and severity of disease [Alexandrov et al., 1996]. However, the low spatial resolution and the inability to calculate absolute blood flow values represent major drawbacks of SPECT. Magnetic resonance imaging with diffusion and perfusion weighting is an intriguing new method to assess tissue viability [Rosen et al., 1989; Kucharczyk, et al., 1993; Knight et al., 1994]. Nevertheless, the relatively high costs and limited clinical availability of MRI in acute stroke warrant the search for alternative diagnostic modalities.

Since a computed tomography (CT) scan of the brain is the first diagnostic imaging study of acute stroke patients, various attempts have been made during the last two decades to establish a CT-based method to calculate rCBF and rCBV [Berninger et al., 1981; Axel, 1981; Nagata and Asano, 1990; Gobbel et al., 1991; Lo et al., 1996; Hamberg et al., 1996]. The widespread availability of CT scanners, together with their high image quality and low costs, are attractive features of this approach. Moreover, by simply extending the routine CT examination, this method would prevent time consuming transport of patients between scanners, further delaying treatment.

Besides the Xenon-based method [Yonas, 1992], the published CT techniques rely on an intravenous bolus injection of a radiographic contrast material and rapid serial ("dynamic") CT scanning to detect the blood flow related changes of the brain tissue

enhancement, or increase in CT number [Axel, 1980]. However, most of these techniques can only provide relative blood flow and blood volume values by side-to-side comparisons of the changes in contrast enhancement with respect to time [Nagata and Asano, 1990; Lo et al., 1996]. This assumes that the contra-lateral side is normal; however, stroke patients rarely have unilateral disease. In the case of bilateral disease, the choice of the reference 'normal' region becomes problematic.

The critical problem in the measurement of absolute rCBF values with contrast enhanced dynamic CT scanning is the calculation of the regional mean transit time (rMTT) through the brain [Gamel et al., 1973; Bronikowski et al., 1983]. The calculation of the rMTT requires the simultaneous measurement of the tissue and the intra-arterial contrast enhancement curves as functions of time after a bolus injection of contrast material [Axel, 1983]. Deconvolution between these two curves gives the MTT in the brain. Due to the limited scanning frequency of the CT scanners in the past (only 1 CT scan every few seconds) and the problem of Partial Volume Averaging (PVA) while scanning small arteries, this method of calculating MTT was of low accuracy [Axel, 1983]. Besides deconvolution, several alternative approaches have been proposed to evaluate the global and regional MTT based on CT scanning, some with promising experimental and clinical results [Gobbel et al., 1991; Steiger et al., 1993; Hamberg et al., 1996]. However, as compared to the more rigorous deconvolution method, these approaches require a number of assumptions that may not be correct in the general case. Further, PVA correction of the imaged cerebral arteries was generally not considered. Using venous blood samples from dynamic CT studies, Lapin et al. [Lapin et al., 1993] showed that PVA may decrease the CT number in a given voxel within a cerebral artery

by as much as four times. This study showed the importance of correcting for PVA when imaging small arteries to obtain accurate arterial contrast enhancement for CT rCBF studies.

By using a slip-ring third generation CT scanner to scan at the rate of one scan per second, we have developed a dynamic CT technique to calculate the rMTT and measure absolute rCBF and rCBV. The objectives of this experimental study were (a) to develop a novel method to correct for PVA, allowing accurate measurement of intra-arterial contrast enhancement curves, and (b) to investigate the accuracy of our CT derived rCBF values in an animal model by comparison to measurements made by the microsphere method.

## 3.3 THEORY

The theoretical basis of our CT CBF measurement technique is the Central Volume Principle, first discussed by Meier and Zieler [1954], and later extended by Roberts and Larson [1973].

### *3.3.1 Central Volume Principle*

Consider a network of capillaries in the brain. The rate of cerebral blood flow into this network is CBF ml/min/g and the cerebral blood volume in it is CBV ml/g. Due to the different possible path lengths that can be followed, blood elements flowing through the network will require different lengths of time (i.e., transit times) to travel from the arterial input to the venous outlet. The average of all possible transit times through this capillary network is the MTT. The Central Volume Principle relates

cerebral blood flow (CBF), cerebral blood volume (CBV), and mean transit time (MTT) in the following simple relationship:

$$CBF = \frac{CBV}{MTT} \tag{3.1}$$

In order to apply the Central Volume Principle, we have to make blood flow detectable by the CT scanner. This is achieved by injecting contrast material into the blood stream. We also assume that a linear relationship exists between the enhancement in CT numbers and the concentration of contrast material within an artery or brain tissue region, and that contrast and blood have the same hemodynamic properties. To describe the response of the CT scanner to contrast material, we also need to introduce two important concepts, the Impulse Residue and the Tissue Residue Functions.

### *3.3.2 Impulse and Tissue Residue Functions*

If X-ray contrast material is injected at the arterial input as a bolus of very short duration (i.e., impulse injection) and the mass of contrast that remains in the capillary network over time is measured with a CT scanner, an enhancement curve of the shape shown in Figure 3.1 will be observed. This is called the Impulse Residue Function, R(t) [Bassingthwaighte et al., 1970].

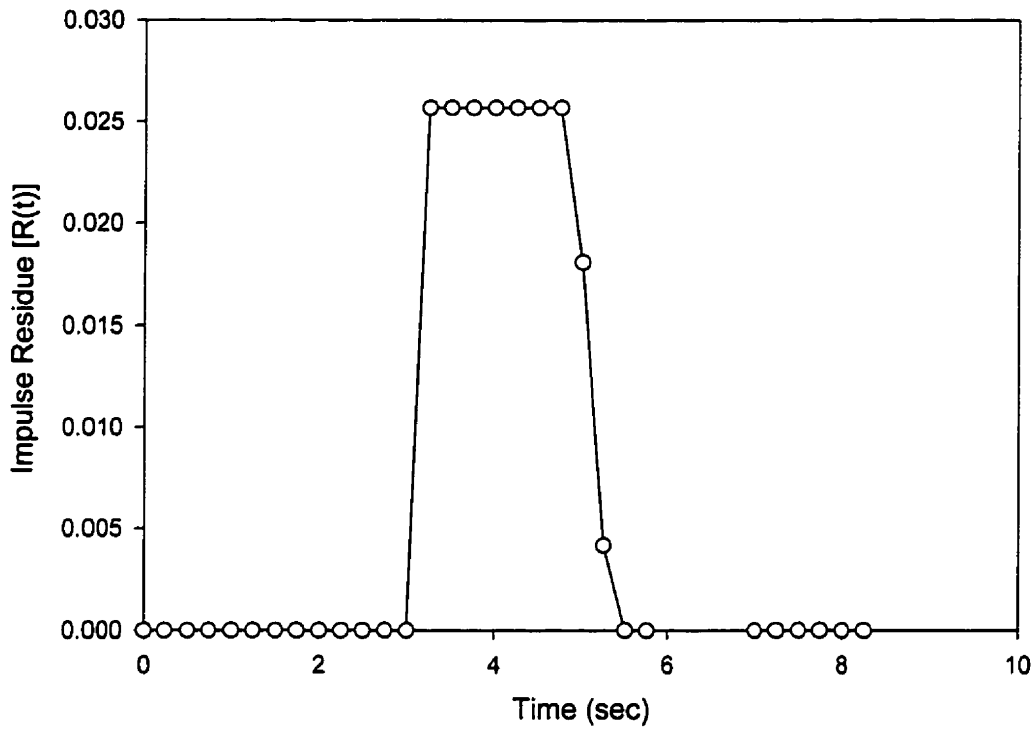


**Figure 3.1. Calculated Tissue Impulse Residue Function in a Rabbit Brain.**
An example of the Impulse Residue Function of the brain, R(t), obtained by deconvolution of $C_a(t)$ and Q(t) in Figure 3.2, illustrating the expected general shape.

The distinguishing features of R(t) are an initial flat plateau followed by a continuous decrease towards the zero baseline (Figure 3.1). The duration of the plateau corresponds to the time interval during which all the injected contrast material remains in the capillary network. Following this time interval, contrast material begins to leave the network leading to the observed drop in R(t).

The significance of the Impulse Residue Function is that it is used to calculate the MTT according to the area over height formula [Axel, 1983]:

$$MTT = \frac{\text{area underneath } R(t)}{\text{height of } R(t) \text{ plateau}} \tag{3.2}$$

The direct experimental determination of R(t) is not possible because it is difficult to identify the specific arterial inlet(s) of a brain region. Even if it were possible, the procedure is highly invasive and would render the method not applicable to patients. Instead, contrast is intravenously injected at a peripheral vein and the mass of the injected contrast material that resides in the capillary network is measured with a CT scanner. The measured function in this case is called the Tissue Residue Function, Q(t). If the enhancement curve at the arterial input is measured to be $C_a(t)$, and if flow is stationary and linear with respect to contrast concentration, then Meier and Zieler [1954] showed that:

$$Q(t) = CBF \times [Ca(t) * R(t)] \tag{3.3}$$

where * denotes the *convolution* operator. In essence, the convolution operation involves the addition of many copies of the same R(t) except for the fact that each copy is multiplied by the arterial contrast enhancement at a different time and then shifted in time by a different amount. In our application of Equation 3.3, we also assume that $C_a(t)$ can be measured at a peripheral artery such as the ear artery.

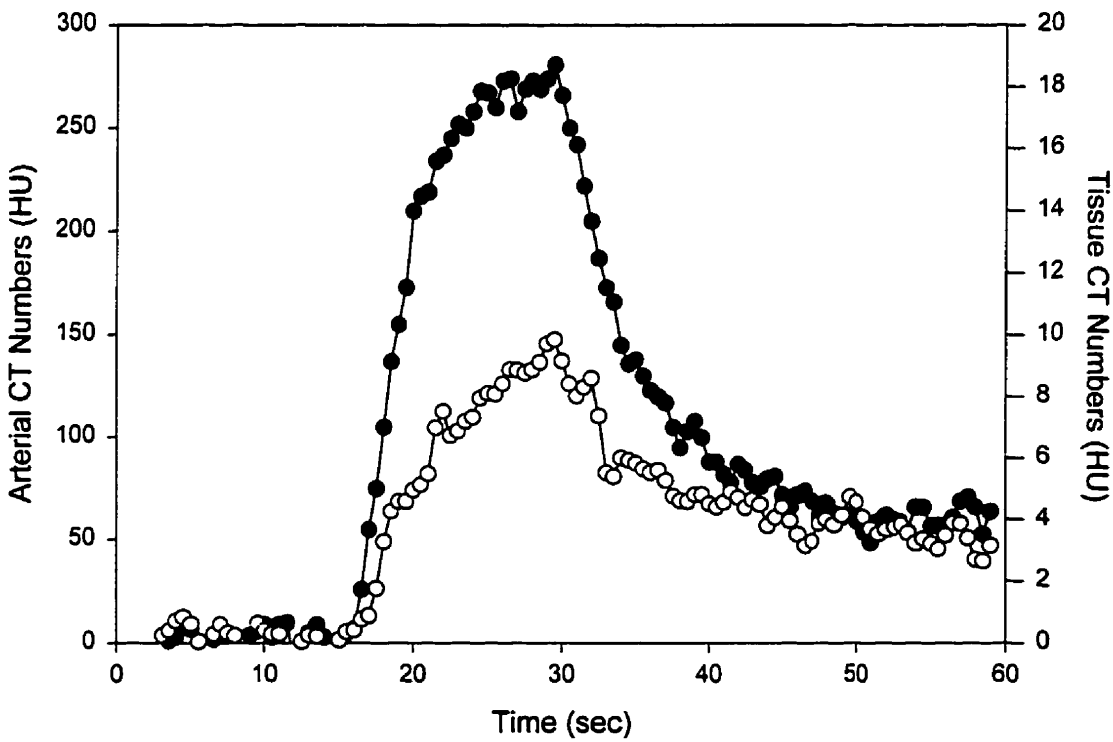


**Figure 3.2. Measured Dynamic CT Contrast Enhanced Curves in a Rabbit Brain.**
Examples of arterial, $C_a(t)$ (closed circles), and regional brain tissue, Q(t) (open circles), contrast enhancement curves obtained from dynamic CT scanning.

### *3.3.3 Deconvolution*

As discussed above, if R(t) and $C_a(t)$ are known, Q(t) can be calculated by their convolution. However, due to experimental limitations as discussed above, R(t) is difficult, if not impossible, to measure. Instead, Q(t) and $C_a(t)$ are measured with the CT scanner (Figure 3.2). The process of calculating R(t), given Q(t) and $C_a(t)$, is the opposite (i.e., inverse) to convolution and is called *deconvolution*. It is known that the deconvolution process is extremely sensitive to noise in the measured arterial and tissue enhancement curves [Gamel et al., 1973; Bronikowski et al., 1983]. Without reliable methods to limit the deleterious effects of noise, the calculated R(t) will be wildly oscillatory, making the calculation of MTT, according to Equation 3.2, impossible.

We have reduced the noise sensitivity of deconvolution using an algorithm previously developed [Yeung et al., 1992] so that solutions of the general shape shown in Figure 3.1 are always produced.

### *3.3.4 Cerebral Blood Volume Calculation*

As discussed by Axel [1980], the volume of flowing blood (i.e., CBV) in a capillary network can be calculated by the ratio of areas:

$$CBV = \frac{\text{area underneath } Q(t)}{\text{area underneath } C_a(t)} \tag{3.4}$$

where Q(t) and $C_a(t)$ are the tissue and arterial enhancement curves, respectively. A typical set of Q(t) and $C_a(t)$ is shown in Figure 3.2. As stated by Axel [1980], this

method is only feasible when the blood-brain-barrier is intact (e.g., normal cerebral tissue) and there is no recirculation of contrast material. In cases where the blood-brain-barrier is compromised (e.g., tumour, infarction, abscess), Q(t) would be a summation of the enhancements due to contrast material in both the intravascular and extravascular spaces, and CBV would be overestimated. To eliminate the effect of recirculation from both $C_a(t)$ and Q(t), we adopted the following procedure: the trailing slope of $C_a(t)$ was extrapolated with a monoexponential function. The extrapolated $C_a(t)$ was then convolved with the calculated R(t) to generate the recirculation corrected Q(t). CBV was calculated as the ratio of the area underneath the recirculation corrected Q(t) to that of the recirculation corrected $C_a(t)$.

## 3.4 METHODS & MATERIALS

### *3.4.1 CT Partial Volume Averaging Correction*

A partial volume phantom was constructed to determine the effect of PVA in imaging small arteries. Figure 3.3 shows a CT image of a cross-section of this phantom. The phantom consisted of one pair of 10 mm diameter tubes (the control tubes), and six pairs of smaller polyethylene (PE) tubes, varying in diameter from 0.76 mm to 2.15 mm (PE60 to PE280). For each pair of tubes, the background tube was filled with distilled water while the contrast tube was filled with a contrast solution (20 mg I/ml) made from the same batch of distilled water. The 10 mm diameter control tubes were large enough so that PVA was negligible. In order to acquire precise CT number measurements, the phantom was scanned 10 times at the same cross-section using the same scanning parameters as in the rabbit studies described below. From the averaged image of these 10

scans, the mean CT number within each tube was obtained by drawing a 2 pixel radius region of interest (ROI) in the center of each tube. The mean CT number in each background tube was then subtracted from the mean CT number in the same size contrast tube to give the enhancement, M, due to the contrast solution for that particular diameter. The partial volume scaling factor (PVSF) for each size of PE tubes was determined as follows:

$$PVSF = \frac{M(\text{control tube})}{M(\text{PE tube})} \tag{3.5}$$

Since the inner diameters of the PE tubes were known, each tube diameter could be correlated to the calculated PVSF value. From this correlation relationship, the PVSF for any other tube diameter can be found.

When imaging an artery with a CT scanner, one does not have any prior knowledge of the artery's diameter; hence, the corresponding PVSF to be used is not known. We developed the following method to provide an estimate of the diameter of an artery. Image profiles (mean CT number plotted against image pixels) of the artery were obtained from a pre-contrast image, and from a contrast enhanced image (when the mean CT number was at its maximum in the vessel ROI). The pre-contrast image profile was subtracted from the enhanced profile to give the background subtracted image profile. A Gaussian curve was fitted to this background subtracted image profile of the artery. The standard deviation (SD) of the Gaussian curve then served as a measure of the imaged artery's diameter.

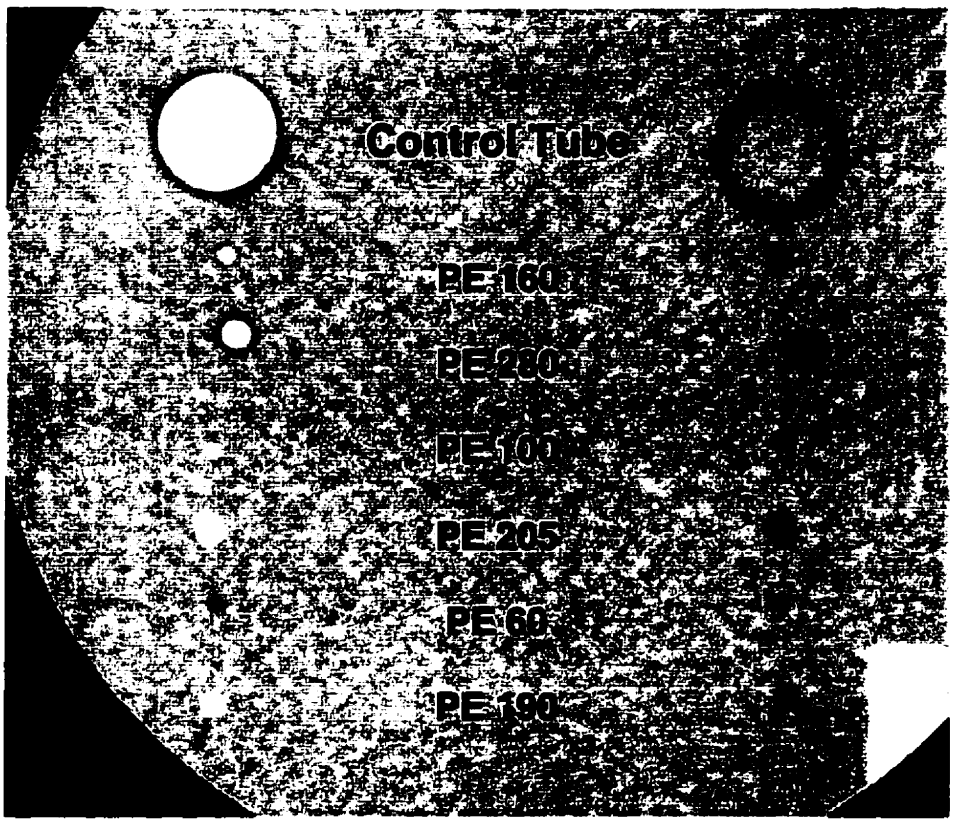


**Figure 3.3. Axial CT Image of the PE Tubes Phantom used to Correct for Partial Volume Averaging.**
PE tubes on the left contain 40 ml of distilled water with 2.7 ml of Isovue 300 (300 mgI/ml contrast) added. PE tubes on the right contain only distilled water to serve as background (ie., non-enhanced). A two pixel radius ROI was drawn in the center of each tube, and the mean CT number was determined within these circular ROIs.

The image profiles of the PE tubes in the phantom were similarly subtracted and fitted with Gaussians. A calibration curve was then generated by correlating the SD value for each PE tube with its associated PVSF value. From the calibration curve, the PVSF for the artery was determined, knowing the SD of the Gaussian fit to its background subtracted image profile. The true $C_a(t)$, corrected for PVA, was the experimentally measured $C_a(t)$ scaled by this PVSF.

### *3.4.2 Animal Protocol*

Six healthy male New Zealand White rabbits were used in experiments approved by the Animal Ethics Committee at The University of Western Ontario. Each rabbit was surgically prepared as follows: mask induction of anaesthesia with halothane, one ear vein was cannulated for administration of muscle relaxant (Vecuronium) during the experiment. Following a tracheotomy, the rabbits were mechanically ventilated to a normocapnic $PaCO_2$ of 40 ± 3 mmHg with a mixture of air and oxygen. Both femoral arteries were catheterized to allow arterial blood sampling for hematocrit and blood gas determination and the measurement of mean arterial pressure (MAP). Both femoral veins were also catheterized for fluid and drug administration if required (e.g., phenylephrine for maintenance of MAP between 75 and 85 mmHg). Isoflurane anaesthesia was then induced at 1 MAC (minimum alveolar concentration). Finally, a thoracotomy was performed with the insertion of a catheter into the left atrial appendage for the injection of fluorescent microspheres required in the *ex-vivo* measurement of rCBF. Local anaesthetic (Lidocaine 1.0%) was administered for all surgical wounds.


**Figure 3.4. Contrast Enhanced Coronal CT Image of a Rabbit Brain.** Two parietal tissue ROI of similar size (left and right) and one central tissue ROI in the basal ganglia were used for all measurements of rCBF. An ear artery (EA) was used to measure the arterial enhancement curve. The post-communicating arteries (in the middle of the brain), and the internal carotid arteries (superior to the optic chiasm) are also visible.

With the surgical procedures completed, the rabbit was placed prone on the patient couch of the CT scanner with its head secured in a head holder. In order to have an ear artery in the same image plane as the brain, a specially designed holder was used to fix the ear horizontally over the rabbit's head (Figure 3.4).

MAP was continuously monitored and rectal temperature was maintained at 38.5 $^{o}$C with a heated, recirculating water-pad and a heat lamp. Hematocrit was measured every 30 minutes.

### *3.4.3 CT Imaging Protocol*

The imaging studies were performed using a slip-ring CT scanner (GE HiSpeed Advantage, Milwaukee, WI, USA). With the slip-ring CT scanner, continuous acquisition of images (i.e., cine scanning) results from the 360$^{o}$ per second unidirectional rotation of the X-ray tube and detector assembly about the gantry. In our scanning protocol, for a total study time of 60 s, 60 rotations were made as the CT couch remained stationary. We have shown that the first cerebral circulation time of intravenously injected contrast material in rabbits is less than 60 s (Figure 3.2); hence, the chosen scan time was sufficient to provide an accurate representation of the arterial and tissue hemodynamics.

The CT imaging protocol involved two steps: the coronal localization scans and the dynamic (cine) CT study scans. For localization, non-enhanced coronal scans were performed at 1 mm intervals, 120 kVp, 80 mAs, 512 × 512 matrix size, 10 cm field of view, and 3 mm slice thickness. From these coronal scans, the image containing the optic chiasm was chosen as the study slice. The optic chiasm served as a marker to

register microsphere rCBF measurements to CT rCBF measurements. Finally, with the level of the optic chiasm localized, a dynamic CT study was performed with the following parameters: 80 kVp, 80 mAs, 512 x 512 matrix, 10 cm field of view, and 3 mm slice thickness. The back projection filter used in the reconstruction of CT images had a cut-off frequency of 10 lp/cm. CT scanning was initiated 5 s before contrast material (Isovue 300, 1.5 ml/kg body wt) was intravenously injected via the cannulated ear vein using an automatic injector (Medrad Injector, Medrad, PA, USA) at the rate of 0.3 ml/s. This delay in contrast material injection allowed for the acquisition of non-enhanced, baseline images. Dynamic CT scanning was maintained during the bolus injection of contrast material and continued for a total of 60 seconds.

From the raw CT projection data, it is possible to retrospectively reconstruct the one second images at arbitrary time intervals. In our studies, to improve time resolution, the time interval between sequential images was set at 0.5 s.

### *3.4.4 Regional CBF Measurements using Fluorescent Microspheres*

In order to validate our CT rCBF measurements, rCBF was also measured using fluorescent microspheres (Interactive Medical Technologies, Los Angeles, CA, USA) as the 'gold' standard. This ex-vivo technique has been used for the past 20 years for validating other rCBF measurement methods [Heymann, et al., 1977]. In our study protocol, rCBF was first measured using the microsphere technique, and then immediately after using the dynamic CT technique. The close spacing in time (time delay < 1 min) ensured that similar hemodynamic conditions existed during both measurement techniques. In addition, arterial blood gases were determined immediately

before and after each rCBF measurement technique to verify that similar $PaCO_2$ levels existed throughout the two measurements. For each microsphere study, fluorescent microspheres (15 μm diameter) of a particular color were randomly selected from a group of six possible colors and injected (1.5 million spheres) into the left atrium. Using a syringe pump, 3.0 ml of blood was withdrawn from a femoral artery at a rate of 1.0 ml/min for three minutes, starting one minute prior to microsphere injection. Upon completion of the experiment, the brain was removed, sectioned into 5 mm thick slices and the slice through the optic chiasm was trimmed to obtain 3 tissue regions corresponding to the same ROIs in the CT images (defined in Section 3.4.6). Regional tissue CBF was then calculated for each tissue sample using the equation:

$$CBF_t = \frac{N_t \times Q}{R} \tag{3.6}$$

where $CBF_t$ is the rCBF of the brain tissue sample in ml/100g/min, $N_t$ is the number of microspheres detected in the tissue sample normalized to 100 g, Q is the rate of aspiration (1.0 ml/min), and R is the total number of microspheres detected in the volume of blood extracted.

### *3.4.5 Repeated Studies*

In 5 out of the 6 rabbits, two or three sequential studies were performed per rabbit. In one rabbit, only one study was completed due to sudden expiration of the subject. The sequential studies were separated by a time interval of at least 30 minutes to

allow for the washout of contrast material from the circulatory system due to the previous injections.

### *3.4.6 CT Data Analysis*

The CT image data was stored on Digital Audio Tape, and then transferred to a SUN *Ultra I* work station for further computational analysis.

For the determination of the tissue residue curve, Q(t), three ROIs in the brain (2 in the parietal regions and 1 in the basal ganglia), as shown in Figure 3.4, were used. These tissue ROIs were drawn such that no major blood vessels were present within them. For those animals that had repeated studies, identical ROIs were used in each of the studies to maintain similar tissue composition and pixel areas in the regions used. Q(t) for each region was obtained by subtracting the regional mean baseline CT number in pre-contrast images from the mean CT number in sequential contrast enhanced images.

The arterial contrast enhancement curve, $C_a(t)$, was determined with a two pixel radius circular ROI in an artery. As shown in Figure 3.4, several arteries were present in the plane of the CT image. The artery used for determining $C_a(t)$ was the one with the largest diameter in the CT image and yielded the highest mean CT number at peak contrast enhancement. This procedure was followed to minimize PVA effects in $C_a(t)$. In most rabbit studies, the ear artery was used. However, in cases when the ear artery was not sufficiently distinct (e.g., when phenylephrine was used to maintain the MAP), one of the cerebral arteries was selected to obtain $C_a(t)$. As in the measurement of Q(t), $C_a(t)$ was also determined by subtracting the mean baseline CT number in the vessel ROI in pre-contrast scans from the mean CT number in contrast enhanced scans. The

background subtracted image profile of the artery was then obtained and fitted with a Gaussian curve. From the SD of the Gaussian, the PVSF of the artery was found and the measured $C_a(t)$ was scaled by this factor to correct for PVA.

### *3.4.7 Statistics*

Statistical analysis was performed using the Jandel Scientific Software Package ('Sigma Plot' and 'Sigma Stat'). Standard descriptive statistics parameters such as mean ± SD values were found. A *t-test* and Mann-Whitney Rank Sum Test were used to compare normally and non-normally distributed data, respectively. One-way ANOVA for repeated measurements was used to determine the variability of the cerebral hemodynamic measurements. Non-linear regression was used to determine the calibration relationship between PVSF and SD of Gaussian fits of the background subtracted image profiles of PE tubes in the partial volume phantom. Linear regression analysis was used to compare the rCBF values derived by the CT and the microsphere techniques. Pearson Product Moment Correlation was used to provide linear correlation coefficients. Statistical significance was declared at the $p < 0.05$ level.

## 3.5 RESULTS

### *3.5.1 CT Partial Volume Averaging Correction*

From a series of CT scans of the partial volume phantom (Figure 3.3), background subtracted image profiles were generated of the cross-sections of the individual tubes. Figure 3.5 shows a typical profile through the center of a given tube of the phantom. Moreover, the Gaussian curve provides an excellent fit for this CT

measured profile. A significant linear correlation was found between the inner diameters and the Gaussian SDs of the imaged PE tubes ($r = 0.998$, $p < 0.001$). This linear relationship was represented by the following regression equation (Figure 3.7):

$$SD = 1.38 + 1.05 \times ID \tag{3.7}$$

where SD is number of pixels, and ID is the inner diameter of a PE tube in mm. This linear relationship confirms the assumption that the Gaussian SD is a reliable measure of the inner diameter of a PE tube imaged in cross-section.

Plotting PVSFs against the Gaussian SDs for the PE tubes in the partial volume phantom (Figure 3.8), we found a significant exponential relationship between the two parameters ($r = 0.996$, $p < 0.001$). From this exponential fit, we derived the following mathematical relationship between the Gaussian SD of a PE tube and its PVSF:

$$PVSF = 1.0 + 2576 \exp(-3.17 \times SD) \tag{3.8}$$

For an imaged artery of unknown inner diameter, its Gaussian SD could be easily obtained by fitting its background subtracted image profile (Figure 3.6), as discussed in Methods & Materials, and the PVSF determined from Equation 3.8. In the rabbit studies, the SDs of the imaged arteries were found to range from 2.4 to 2.8, and the corresponding PVSFs from Equation 3.8 were between 2.3 to 1.4.

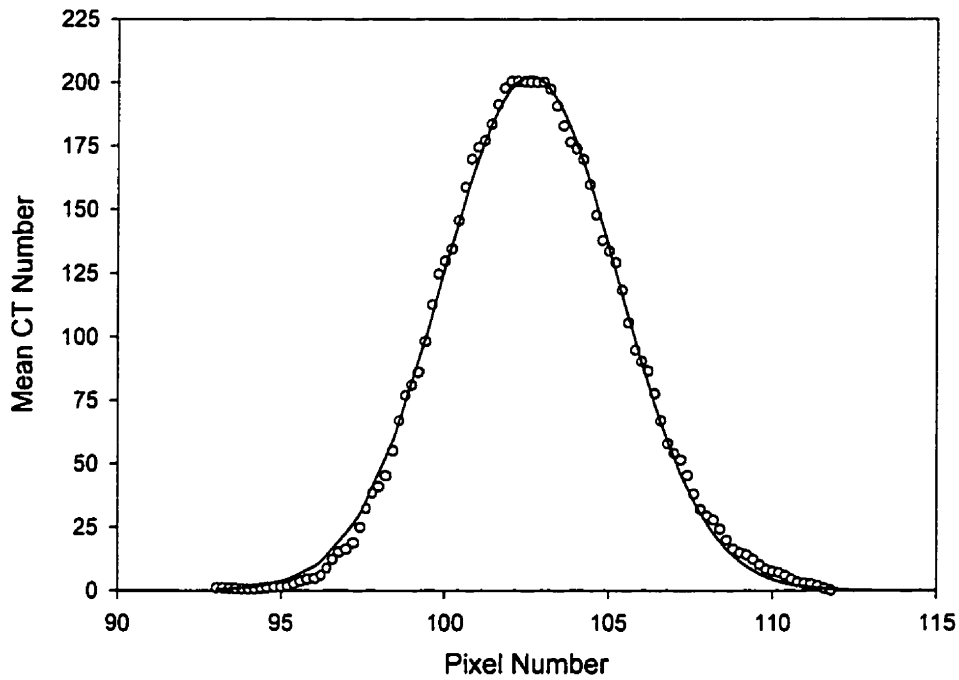


**Figure 3.5. Background Subtracted Image Profile of a PE-160 Tube with the Fitted Gaussian Curve.**
The calculated Gaussian SD was 2.58 for the known tube inner diameter of 1.14 mm.

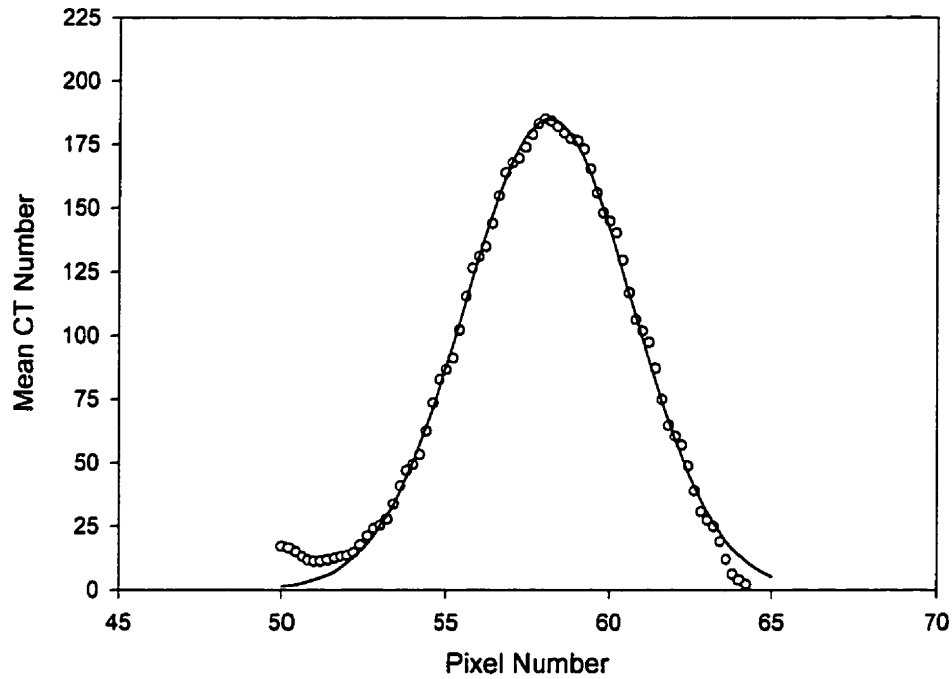


**Figure 3.6. Background Subtracted Image Profile of a Rabbit Ear Artery with the Fitted Gaussian curve.**
The calculated Gaussian SD was 2.58 for the CT imaged ear artery corresponding to an estimated inner diameter of about 1.14 mm for the ear artery.

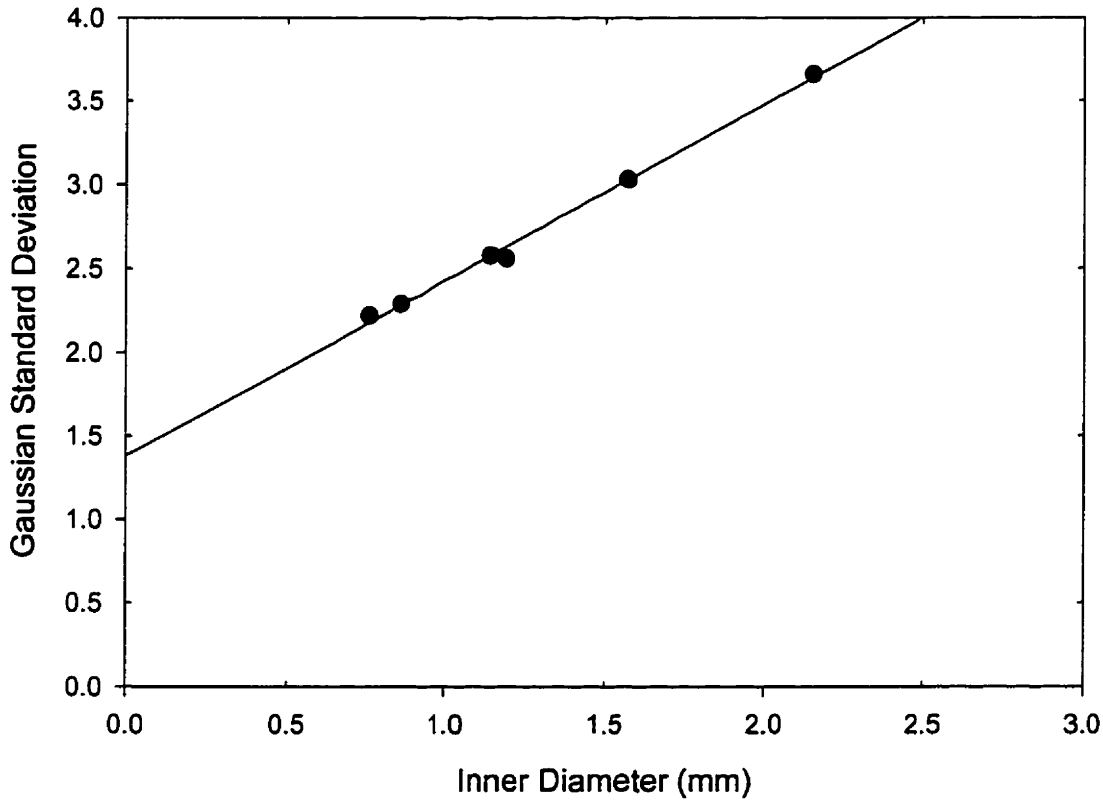


**Figure 3.7. PE Tubes Phantom Experiments: Inner Diameter versus. Gaussian Standard Deviation (SD).**
There was a significant linear correlation between the Gaussian SDs and the inner diameters of the PE tubes ($r = 0.998$, $p < 0.001$).

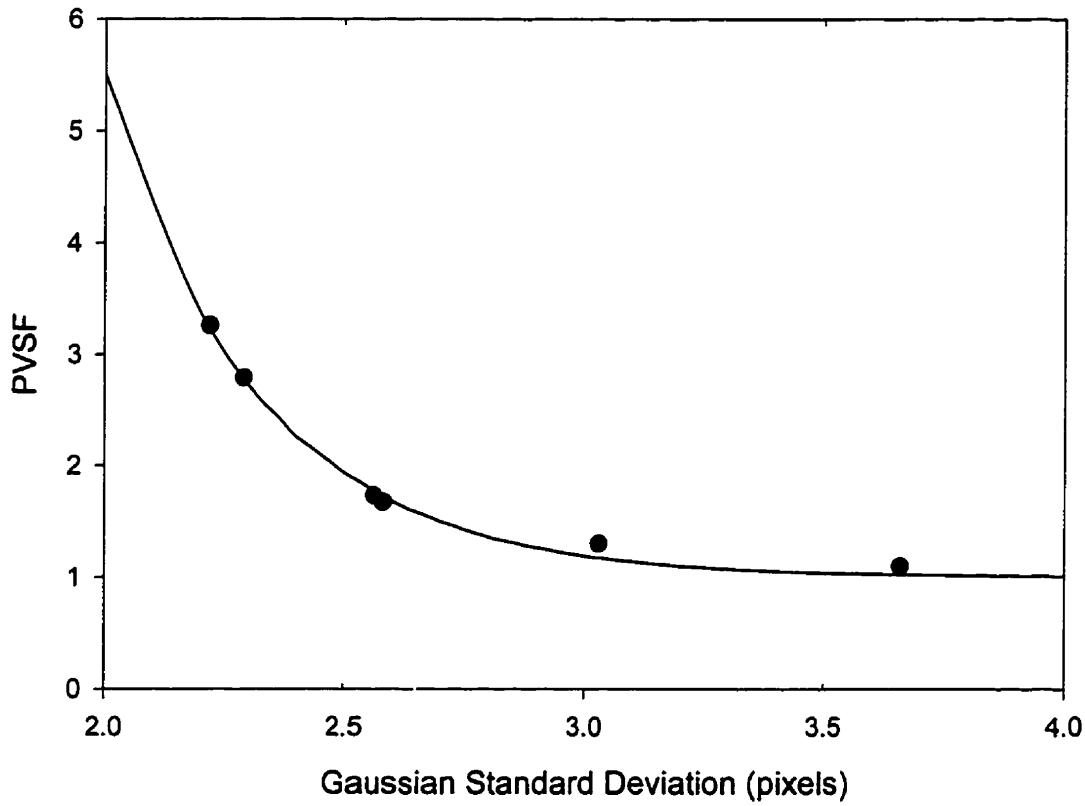


**Figure 3.8. PVSF Calibration Curve obtained from the PE Tubes Phantom.** A significant exponential correlation was found between PVSF and Gaussian SDs for the PE tubes ($r = 0.996$, $p < 0.001$).

### *3.5.2 Regional CBF and CBV Measurements in Rabbits*

Details of the monitored physiological parameters for the 6 rabbits are listed in Table 3.1. Using paired t-test, no statistically significant change ($p > 0.1$) was found in the physiological parameters over the duration of the repeated studies. However, due to the withdrawal of intravenous and arterial blood samples over time, a slight decrease in hematocrit was observed (Table 3.1).

The mean regional values (± SD) of the measured hemodynamic parameters for both the dynamic CT and the microsphere methods are listed in Table 3.1. A comparison of the dynamic CT rCBF values with those determined using the 'gold' standard (microsphere) method revealed a significant correlation ($r = 0.837$, $p < 0.001$) between the two methods (Figure 3.9). The accuracy of the dynamic CT method to measure rCBF compared well with the microsphere method as shown by the near unity regression slope of Figure 3.9 (slope = $0.97 \pm 0.03$).

Table 3.2 compares the reproducibility of the microsphere method and the dynamic CT method in measuring rCBF under steady state conditions. The variability for each method was determined by comparing rCBF in identical ROIs from the repeated studies using ANOVA. The variability was approximately 9 % higher for the CT rCBF values in comparison to the microsphere data. The differences in the CT measurements in the repeated studies, however, did not reach statistical significance ($p > 0.10$). The variability for the CT rCBV values was better at 15.5 % and again there was no statistically significant difference in the repeated measurements ($p > 0.10$).

**Table 3.1. Monitored Physiologic and Measured Cerebral Hemodynamic Parameters.** Values are Mean ± SD, and N is the number of regional measurements. Three regional measurements were made per study.

| | Study 1 (N=18) | Study 2 (N=15) | Study 3 (N=6) | Total (N=39) |
|---|---|---|---|---|
| Physiologic Parameters | | | | |
| PaCO2 (mmHg) | 40.4 ± 3.3 | 39.1 ± 4.0 | 39.3 ± 1.7 | 39.7 ± 3.3 |
| MAP (mmHg) | 79.6 ± 9.0 | 77.1 ± 7.8 | 72.5 ± 0.2 | 77.6 ± 7.8 |
| Temperature (°C) | 38.9 ± 0.4 | 38.9 ± 0.5 | 38.4 ± 0.8 | 38.8 ± 0.5 |
| Hematocrit | 35.9 ± 1.1 | 34.1 ± 1.3 | 33.3 ± 1.8 | 34.8 ± 1.6 |
| Dynamic CT Parameters | | | | |
| rCBV (ml/100g) | 2.14 ± 0.82 | 1.89 ± 0.69 | 1.42 ± 0.19 | 1.93 ± 0.74 |
| rMTT (sec) | 1.88 ± 1.20 | 1.72 ± 0.92 | 1.85 ± 0.86 | 1.81 ± 1.02 |
| rCBF (ml/min/100g) | 77.1 ± 30.1 | 76.8 ± 34.4 | 53.5 ± 24.3 | 73.3 ± 31.5 |
| Microsphere Parameters | | | | |
| rCBF (ml/min/100g) | 76.1 ± 33.4 | 80.3 ± 33.5 | 54.0 ± 4.8 | 74.3 ± 31.6 |

**Table 3.2. Comparison of the reproducibility of dynamic CT with microsphere rCBF measurements in repeated studies (N=15) and in hemispheric (right and left) measurements (N=13).** The percent variability was determined using an ANOVA for repeated measurements. Percent difference was calculated as 100×[2×(right – left)]/(right + left). # denotes no statistically significant difference ($p > 0.10$) as determined by *t-test*, or Mann-Whitney Rank Sum Test.

| Method and Hemodynamic Parameter | Variability for Repeated Measurements (%) | Right-Left Hemisphere Percent Difference (%) |
|---|---|---|
| Microsphere rCBF (ml/min/100g) | 23.5 | 3.2# |
| CT rCBF (ml/min/100g) | 32.5 | 1.9# |
| CT rCBV (ml/100g) | 15.5 | 8.4# |

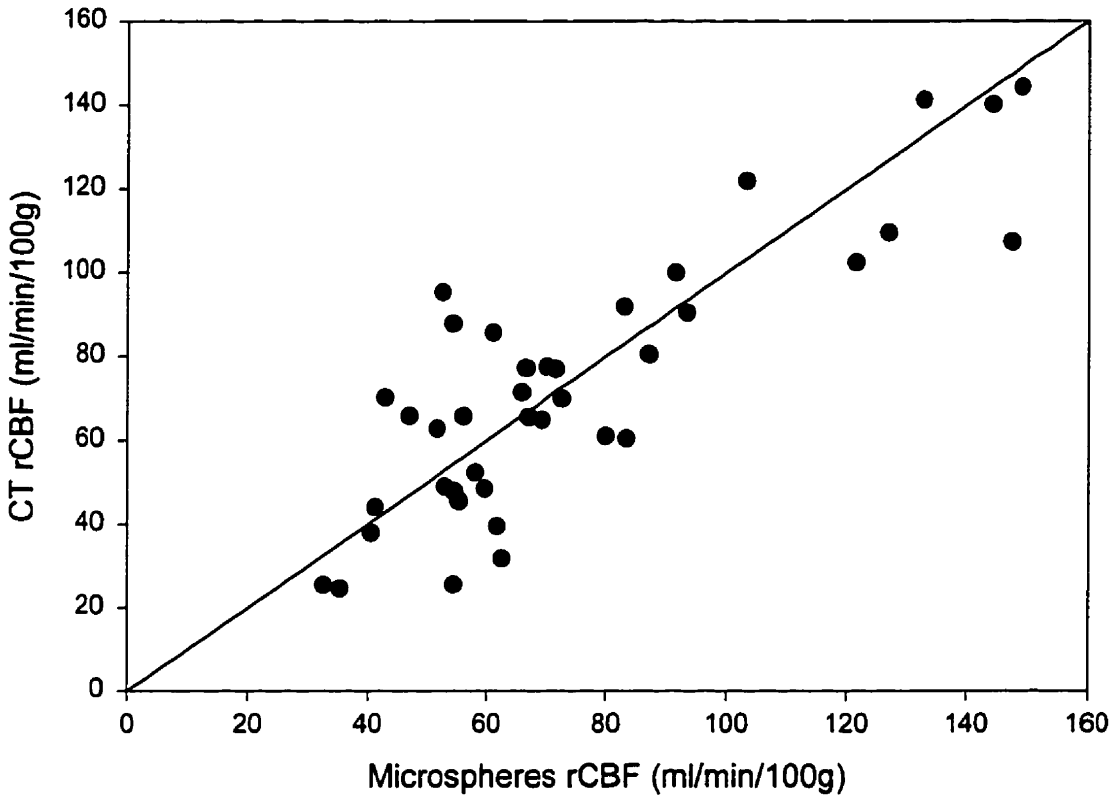


**Figure 3.9. Dynamic CT Meaurements plotted against Microspheres Measurements of rCBF (ml/min/100g) for N=39 ROIs.**
There was a strong correlation between these two sets of measurements ($r = 0.837$, $p < 0.001$). The slope of the regression line ($0.97 \pm 0.03$) was close to unity.

The side-to-side comparison of the hemispheric rCBV and rCBF values revealed only minor differences (Table 3.2). However, a *t-test* analysis revealed no statistically significant difference in the dynamic CT as well as in the microsphere measurements between contra-lateral hemispheres ($p > 0.10$).

## 3.6 DISCUSSION

### *CT Partial Volume Averaging Correction*

In CT, PVA results from the limited spatial resolution of the scanner and decreases with increased spatial resolution. Since the spatial resolution of the CT scanner used in these studies is 10 lp/cm, PVA remains an inherent source of error when imaging small blood vessels. As stated by Axel [1980], because of PVA, the enhancement in small blood vessels cannot be accurately measured with CT, since their volume is averaged together with that of surrounding tissue. Due to the much lower attenuation coefficient of the extravascular tissue, the mean CT number -- reflecting the contrast concentration -- within the arterial ROI will be considerably underestimated. Hence, a falsely lower arterial enhancement curve would be measured, which would result in overestimation of rCBV and of rCBF.

In our study, we have demonstrated that the SD of the Gaussian that fits the background subtraced image profile of an artery imaged in cross-section (Figure 3.6) is linearly related to the diameter of the artery (Equation 3.7). Also, for each diameter, a PVSF can be determined to correct for the effect of PVA in the measurement of contrast enhancement (Equation 3.8). In the dynamic CT studies, PVSFs for the rabbit ear arteries had a mean of 1.7. Thus, without PVA correction, the arterial enhancement

curve would have been underestimated, on the average, by approximately 60 %, resulting in a similar overestimation of the CT rCBV and rCBF values, respectively. Based on our phantom studies, when imaging an artery with an internal diameter greater than 1.73 mm (or Gaussian SD > 3.2), the effect of PVA in the measurement of contrast enhancement is negligible.

However, limitations of this method must be recognized. First, it only provides an approximate correction for the PVA effect, allowing the resulting measurement error to be reduced without completely eliminating it. Secondly, in our rabbit studies, we selected only those arteries for PVA correction that appeared to be approximately at right angles to the scan plane. In cases where the artery is at an oblique angle to the CT scan plane, a higher Gaussian SD could be expected, resulting in an inappropriate PVA correction factor being used. This would lead to slightly higher rCBV and rCBF measurements. Thus, we recommend applying our method only for those vessels that appear as symmetric circles on the CT image.

In summary, we have developed a convenient method to correct for PVA when imaging small arteries. In contrast to Lapin et al. [Lapin et al., 1993], our method does not require any intravenous blood sampling, post-study scans of these blood samples, and CT scans of the subject ten minutes post-contrast infusion. Our convenient method has potential to overcome the problem of PVA in various clinical and experimental settings in which accurate measurements of the intravascular contrast concentration are needed.

***Dynamic CT Measurements of CBF and CBV***

The second part of this study was aimed at validating our dynamic CT rCBF measurements using a well-established technique (i.e., microspheres) in a normal animal model. To the best of our knowledge, this is the first experimental study to validate a deconvolution based approach in the CT measurement of rCBF since the original description by Axel over a decade ago [Axel, 1983].

A strong correlation was found between the dynamic CT and the fluorescent microsphere rCBF measurements ($r = 0.835$, $p < 0.001$). This correlation compares well with others who have validated their dynamic CT [Gobbel et al., 1991] and stable Xenon-CT [Dewitt et al., 1989] techniques with microsphere measurements. Using the "center of gravity" of the dynamic contrast enhancement curves to obtain rMTT values for rCBF measurements in dogs, Gobbel et al. [1991] showed a strong correlation ($r=0.95$) in the hemisphere and basal ganglia ROIs, but a poor correlation in the internal capsule ($r = 0.51$). With regards to the stable Xenon-CT method, Dewitt et al. [1989] revealed a correlation of 0.69 in 7 baboons under conditions of normocapnia and 0.83 in 5 baboons for both hypocapnia and hypercapnia (20 and 60 mmHg, respectively). Our mean rCBF values are similar to those obtained by other investigators in rabbits under isoflurane anaesthesia [Patel and Mutch, 1990; Todd et al., 1994]. Our results further indicate that rCBF can be measured in ROIs as small as 0.38 $cm^2$ in rabbits using 80 mAs per CT scan at 80 kVp for 60 scans and a contrast dose of 1.5ml of Isovue 300 per kilogram body weight.

The short-term reproducibility of our rCBV and rCBF measurements was approximately 15% and 30%, respectively (Table 3.2). The good rCBV precision (Table

3.2) is similar to others reporting variabilities of 14% in rabbits [Hamberg et al., 1996] and 20% in humans [Steiger et al., 1993]. In contrast to the CT rCBV measurements, the precision of our CT rCBF method was lower. The fact that the variability of the microsphere results was also approximately 25 % suggests that this could, in part, reflect true physiological changes due to the 30 minutes inter-study delay between repeated studies. However, a similarly low rCBF precision was found by Gobbel et al. in repeated canine studies using only 10 min intervals [Gobbel et al., 1991]. Thus, part of this variability in our CT rCBF measurements is presumably due to methodological issues. Such low precision may have resulted from the inaccuracy of the rMTT calculations due to the inherent noise sensitivity of deconvolution [Gamel et al., 1973; Bronikowski et al., 1983; Axel, 1983]. In particular, the deconvolution of noisy tissue and arterial enhancement curves may produce impulse residue functions not characteristic of the capillary bed, resulting in considerable rMTT errors. Since enhancement is linearly related to the amount of intravascular iodine [Fike et al., 1982], a better signal-to-noise ratio can be obtained by either increasing the iodine concentration in the contrast material (> 300 mg I/ml) or increasing the infusion rate (0.3 ml/s in our studies) of the contrast material.

Nevertheless, an advantage of our deconvolution method is that it allows for rMTT calculations without curve-fitting and other modifications to the originally measured enhancement curves. Since the first and subsequent passage of the bolus is inherent in the arterial as well as the tissue enhancement curves, the simultaneous imaging of an artery in the same tissue plane excludes recirculation as a potential source of error in the calculation of rMTT. Furthermore, ROI specific MTT values can be

calculated using our approach in comparison to global values used by other investigators [Hamberg et al., 1996]. This is of particular importance in pathological situations (e.g., stroke) where different and inhomogeneous rMTT values could exist between normal and ischemic regions.

The radiation dose associated with our dynamic CT method must also be considered. Although the number of images required for a dynamic CT study is about 3 times greater than a conventional head scanning protocol (60 vs. 17 scans), much lower X-ray tube parameters are used (80 kVp and 80 mA vs. 120 kVp and 340 mA) [Atherton and Huda, 1996]. Thus, the same effective dose equivalent of approximately 1.5 mSv [Atherton and Huda, 1996] is delivered with our dynamic CT protocol. However, the effective dose equivalent of other blood flow measurement techniques, such as PET and SPECT, is more than double this value [Huda and Sandison, 1990; 1989]. At present, our technique is limited to a single slice within the brain. In stroke, it is uncertain whether this single slice approach is sufficient for diagnostic purposes. It is further unclear which slice has to be used to obtain useful prognostic information. The introduction of multi-slice CT scanners in the future may overcome this limitation. However, the increased radiation risk due to the higher dose of multi-slice studies must be weighed against the additional clinical benefit. Moreover, movements of the subject may occur during the dynamic CT scanning interval. Although the scanning time of 60 s in our dynamic CT study is much shorter than that of Xenon-CT, PET, and SPECT studies, movement artifacts (especially in the longitudinal direction) remain an important problem that affects the accuracy of our hemodynamic measurements. Thus, the feasibility of our technique for critically ill patients, who are unable to remain still, has yet to be evaluated.

Finally, we validated our CT rCBF method for a wide physiological range between 30 and 150 ml/min/100g (Figure 3.9). For rCBF < 30 ml/min/100g, as found in ischemic tissue, the accuracy and reproducibility still have to be determined.

## 3.7 CONCLUSIONS

In conclusion, we have validated a new and convenient dynamic CT method to measure rCBF. The widespread availability of CT scanners, coupled with their low operating costs and the high temporal and spatial resolution of CT scans, suggests that our method can serve as an alternative diagnostic tool to assess the cerebral hemodynamics in various experimental and clinical situations.

# 4.0 SUMMARY AND FUTURE WORK

## 4.1 SUMMARY OF THESIS

First, this thesis presented the implementation and improvements of a previously developed [Yeung et al., 1994] *in-vivo* method of measuring cerebral blood volume (CBV) using contrast enhanced CT and a two compartment model of the brain. This method was applied in a rabbit brain tumour model to examine the individual effects of Propofol and Isoflurane anaesthesia on hyperventilation induced changes on regional CBV and cerebral blood flow (CBF). In comparison to previous investigators [Yeung et al., 1994; Howard, 1996], arterial contrast enhancement curves were obtained from scanning arteries (e.g., radial, ear) in the same plane of the brain images thus avoiding the invasive procedure of in-line arterial blood sampling. Second, this thesis described the development and implementation of a new *in-vivo* method of measuring regional CBF using contrast enhanced CT through the application of the Central Volume Principle and a deconvolution technique. This method was applied and validated in a normal rabbit model against the *ex-vivo* 'gold' standard method of microspheres. The following is a summary of this thesis:

(1) Regional *in-vivo* CBV and *ex-vivo* CBF measurements were made simultaneously in two groups of eight brain tumour rabbits which were administered either Propofol or Isoflurane anaesthesia. It was found that when hyperventilation was induced during Propofol anaesthesia, there was a significant decrease in both CBV and CBF ($p < 0.05$) in the peri-tumour region only. The percent change in CBV was less than that of CBF in this region upon hyperventilation. The tumour, contra-lateral and left temporal normal

regions all revealed no statistically significant change in either CBV or CBF ($p >> 0.05$) upon hyperventilation. When hyperventilation was induced during Isoflurane anaesthesia, there was a significant global decrease in CBV ($p < 0.05$) and no significant decrease in CBF ($p >> 0.05$) in all the regions examined except the left temporal normal region ($p < 0.05$). The percent change in CBF was greater than that of CBV in this normal region upon hyperventilation. In comparing the vasoactive effects of anaesthesia induction on CBV and CBF at normocapnia, Propofol regional CBV and CBF values were significantly smaller than for Isoflurane anaesthesia. Moreover, a comparison of regional CBV measurements made at normocapnia with Propofol and measurements made at hypocapnia with Isoflurane revealed that Propofol anaesthesia induced significantly lower CBV values ($p < 0.01$) in only the left temporal lobe, while there were no significant differences in the other regions examined ($p >> 0.05$). The time control studies revealed no significant change in both CBV and CBF ($p >> 0.05$) as a result of the duration of either Propofol or Isoflurane anaesthesia.

(2) The purpose of Chapter 3 was two-fold: i) to develop a method to correct for the effect of partial volume averaging (PVA) in the CT measurement of contrast enhancement in small arteries, and ii) to validate a dynamic contrast enhanced CT method for the measurement of regional cerebral blood flow (rCBF). Contrast enhanced CT scans of tubes of known inner diameters were performed to estimate the size dependent scaling factors (PVSF) due to PVA. The background subtracted image profiles of the contrast filled tubes were fitted to Gaussians, and the standard deviations (SDs) of these curves were correlated with the PVSF of each tube. In the second part of

the study, 13 studies were performed in six New Zealand White rabbits under normal conditions. Dynamic CT measurements of rCBF, regional cerebral blood volume (rCBV) and regional mean transit time (rMTT) were calculated in the left and right parietal lobes, and the basal ganglia. The CT rCBF values were compared to those obtained by the 'gold' standard microsphere method. We found strong correlations ($r > 0.95$) of the SDs of the Gaussian curves to (a) the known tube inner diameters and (b) their size related PVSF. These correlations demonstrated that the error from PVA in the measurement of arterial enhancement could be corrected without knowledge of the actual size of the artery. The animal studies revealed a mean (± SD) rCBF of 73.3 ± 31.5 ml/100g/min, a mean rCBV of 1.93 ± 0.74 ml/100g, and a mean rMTT of 1.81 ± 1.02 s. A strong correlation was found between rCBF values derived by the CT and the microsphere methods ($r = 0.835$, $p < 0.001$, slope = 0.97 ± 0.03). We have validated a new dynamic CT method to measure rCBF in a normal rabbit model. The accuracy of this technique suggests that it can be used as an alternative diagnostic tool to assess the cerebral hemodynamics in experimental and clinical situations.

## 4.2 FUTURE WORK

### *4.2.1 CT CBF Measurements in Tissue with Finite Blood-Brain-Barrier Permeability*

In most neurological disorders (e.g., tumour), the blood-brain-barrier (BBB) is compromised leading to extravasation of contrast material into the extravascular space (EVS). In such cases, using the CBV calculation method described in Chapter 3 would lead to overestimated CBV measurements, hence application of the Central Volume Principle would lead to overestimated CBF values. Thus, in order to apply our dynamic

CT CBF method in tissue with finite capillary permeability, leakage of contrast material across the BBB must be accounted for in the application of the Central Volume Principle. The following section describes a novel theoretical approach [Singal et al., 1997] that extends the Central Volume Principle to tissue with finite BBB permeability. This section is then followed by a proposed validation study to verify our dynamic CT method and application of this extended principle to a rabbit brain tumour model.

*4.2.1.1 Theory*

As stated in Chapter 3, the same assumptions with respect to linearity and stationarity of the injected contrast material are considered. When leakage of contrast material into the EVS occurs, the path lengths followed by the contrast molecules through the capillary network can be classified as those that remain entirely intravascular, and those that leak into the EVS and then diffuse back into the intravascular space (IVS). Let $R_i(t)$ denote the impulse residue function (IRF) for the contrast molecules remaining in the IVS, and $R_e(t)$ denote the IRF for contrast molecules that leak across the BBB into the EVS. If E is the extraction fraction (i.e., the fraction of contrast that leaks into the EVS from the IVS), then the tissue IRF is given by:

$$R(t) = ER_e(t) + \{1 - E\}R_i(t) \qquad (4.1)$$

where the IRFs in Equation 4.1 are all scaled by CBF. As shown from Equation 3.3 (as defined in Chapter 3), these CBF-scaled IRFs are calculated from the deconvolution of the measured arterial, Ca(t), and tissue, Q(t), enhancement curves. Figure 4.1 provides a

schematic representation of Equation 4.1 and demonstrates a typical tissue IRF, R(t), measured in tissue with a compromised BBB. The initial plateau of R(t) (with height equal to CBF) is followed by a progressive decrease to a second plateau. This second plateau, which is lower in height but much longer in duration than the first plateau, occurs due to the slow back-diffusion of contrast material into the IVS from the larger EVS volume [St. Lawrence and Lee, 1998]. The first plateau represents the passage of contrast material through the IVS of the tissue. The duration of this plateau represents the minimum transit time in which the entire injected volume of contrast material remains within the tissue (i.e., in both the IVS and EVS). After this minimum time, contrast material begins to wash out from the tissue region corresponding to the progressive decrease in R(t). However, in the case where a finite BBB permeability exists, a fraction, E, of contrast material will leak into the EVS. This fraction in the EVS remains visible to the CT scanner until it returns to the IVS (via back diffusion) and is eventually cleared by the CBF. Thus, as shown in Figure 4.1, the second plateau of R(t) represents the EVS fraction (or the EVS IRF, $R_e(t)$). The value of the fraction is given by:

$$E = \frac{B}{A} \tag{4.2}$$

where A and B are the heights of the second and first plateau of R(t), respectively. Furthermore, as shown in Figure 4.1, by extapolating the EVS plateau to time zero and subtracting it from R(t), the CBF-scaled IRF, $R_i(t)$, for the IVS is obtained.

From the Central Volume Principle, the tissue mean transit time (MTT) for the IVS is given by:

$$MTT = \frac{CBV}{CBF} \tag{4.3}$$

As shown in Chapter 3, the MTT is calculated from the determined Ri(t) using:

$$MTT = \frac{\text{area under } R_i(t)}{\text{max height of } R_i(t)} \tag{4.4}$$

where $R_i(t)$ is equal to the tissue IRF, R(t), when the BBB is intact (i.e., no leakage of contrast material across the BBB).

However, in the case of a finite permeable BBB (as shown in Figure 4.1), the height of $R_i(t)$ is given by:

$$R_i(0) = \{1 - E\}CBF \tag{4.5}$$

where $R_i(0)$ is the maximum height of the extrapolated $R_i(t)$ at time zero. Thus, substituting Equation 4.5 into Equation 4.4, the MTT is given by:

$$MTT = \frac{\int_0^\infty R_i(t)dt}{\{1 - E\}CBF} \tag{4.6}$$

Substitution of Equation 4.6 into Equation 4.3 yields:

$$CBV = \frac{\int_0^\infty R_i(t)dt}{1-E} \tag{4.7}$$

where Equation 4.7 accounts for the BBB permeability in the calculation of CBV.

In order to measure CBF in tissue with a finite BBB permeability, the following protocol is used. First, dynamic CT measurements of the tissue, Q(t), and arterial, $C_a(t)$, contrast enhancement curves are obtained. Using our deconvolution algorithm, the tissue IRF, R(t), is obtained from the measured Q(t) and $C_a(t)$ curves. From this calculated R(t), the intravascular IRF, $R_i(t)$ is determined by extrapolation as discussed above. Hence, from Equation 4.7, CBV can be calculated. From Equations 4.4 and 4.6, the CBF can then be determined using:

$$CBF = \frac{R_i(0)}{1-E} \tag{4.8}$$

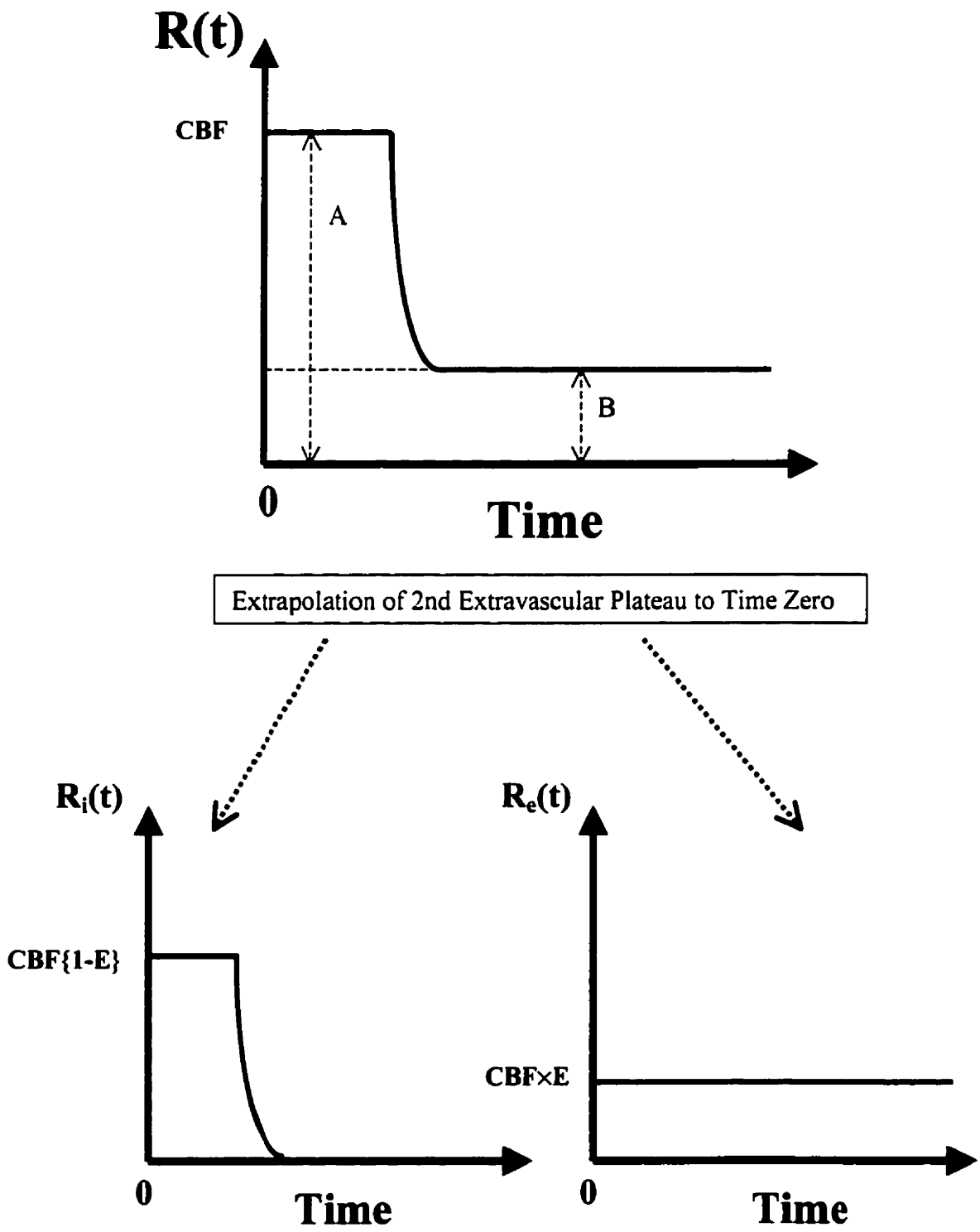


**Figure 4.1. Separation of a CBF-scaled Tissue Impulse Residue Function into its Intravascular, $R_i(t)$, and Extravascular, $R_e(t)$, Components.**
The extraction efficiency (E) of the contrast material is the ratio of heights B to A.

*4.2.1.2 Validation of CT CBF Measurements in a Rabbit Brain Tumour Model*

The above theoretical approach will be applied to determine the accuracy of regional CBF measurements in tissue regions with compromised BBB (e.g., tumour and peri-tumoural tissue). Since the tissue enhancement curves, Q(t), for these regions and the arterial enhancement curve, Ca(t), exist from the rabbit brain tumour studies of Chapter 2, we will apply our deconvolution algorithm to these curves to calculate the regional tissue IRFs. From these tissue IRFs, the analysis method presented above will be used to determine regional CBV and MTT, hence regional CBF. These regional CBF values will then be correlated to the microsphere CBF values previously obtained for these pathological regions in the anaesthesia studies of Chapter 2. From this correlation, the accuracy of our dynamic CT method to measure regional CBF in tissue with finite capillary permeability will be evaluated.

### *4.2.2 The Comparative Anaesthetic Effects of Propofol and Isoflurane on CBV and CBF during Hyperventilation in Patients with Intracranial Tumours*

Validating our dynamic *in-vivo* CT CBF technique in a rabbit brain tumour model will allow us to implement our method in the assessment of regional CBV and CBF in patients with intracranial tumours. The goal of this project is to repeat the anaesthesia studies of Chapter 2 in humans. Changes in regional CBV and CBF in patients with brain tumours during Propofol or Isoflurane anaesthesia with and without hyperventilation will be measured. For each condition, the percent change in CBV and CBF in the tumour region will be compared with the corresponding contra-lateral normal brain region. Our study will aid anaesthetists both in the operating room and the Intensive Care Unit to identify anaesthetics that either blunt or amplify the response of

CBV to $PaCO_2$ in the effort to modify ICP. Moreover, this study will contribute to a better understanding of how $PaCO_2$ and anaesthetics affect the relationship between CBV and CBF in patients with brain tumours. Ultimately, this study should provide some useful insight in helping anaesthetists make a more rational choice of anaesthetic in patients with raised ICP due to intracranial lesions.

## REFERENCES

Adams HP, Brott TG, Furlan AJ, et al.: Guidelines for thrombolytic therapy for acute stroke: A supplement to the guidelines for the management of patients with acute ischemic stroke. Stroke 27:1711-1718, 1996.

Alexandrov AV, Black SE, Ehrlich LE, et al.: Simple visual analysis of brain perfusion on HMPAO SPECT predicts early outcome in acute stroke. Stroke 27:1537-1542, 1996.

Artru AA: Reduction of cerebrospinal fluid pressure by hypocapnia: changes in cerebral blood volume, cerebrospinal fluid volume, and brain tissue water and electrolytes. J Cereb Blood Flow Metab 7(4): 471-9, 1987.

Atherton JV, Huda W: Energy imparted and effective doses in computed tomography. Med Phys 23:735-741, 1996.

Axel L: Cerebral blood flow determination by rapid-sequence computed tomography. A theoretical analysis. Radiology 137:679-686, 1980.

Axel L: A method for calculating brain blood flow with a CT dynamic scanner. Adv Neurol 30:67-71, 1981.

Axel L: Tissue mean transit time from dynamic computed tomography by a simple deconvolution technique. Invest Radiol 18:94-99, 1983.

Bassingthwaighte JB, Chinard FP, Crone C, Lassen NA, Perl W: Definitions and terminology for indicator dilution methods. In: Crone C, Lassen NA, eds. Capillary Permeability, pp. 665-669. Copenhagen: Munskgaard, 1970.

Blasberg RG, Fenstermacher JD, Patlak CS: Transport of α-aminoisobutyric acid across brain capillary and cellular membranes. J Cereb Blood Flow Metab 3:8-32, 1983.

Berninger WH, Axel L, Norman D, Napel S, Redington RW: Functional imaging of the brain using computed tomography. Radiology 138:711-716, 1981.

Bronikowski TA,. Dawson CA, Linehan JH: Model-free deconvolution techniques for estimating vascular transport functions. Int J Biomed Comput 14:411-429, 1983.

Carson BS, Anderson JH, Grossman SA, Hilton J, White CL, Colvin OM, Clark AW, Grochow LB, Kahn A, Murray KJ: Improved rabbit brain tumor model amenable to diagnostic radiographic procedures. Neurosurgery 11(5): 603-608, 1982.

Cenic A, Lee T-Y, Craen RA, Gelb AW: A helical CT study of cerebral perfusion and related hemodynamic parameters. SPIE Proceedings Vol. 3033, Medical Imaging 1997: Physiology and Function from Multi-Dimensional Images, pp. 257-267, 1997.

Cenic A, Lee TY, Craen RA, Gelb AW: Dynamic contrast-enhanced X-ray CT measurement of cerebral blood volume in a rabbit tumour model. SPIE Proceedings Vol. 3337, Medical Imaging 1998: Physiology and Function from Multi-Dimensional Images, pp. 253-262, 1998.

Cenic A, Nabavi DG, Craen RA, Gelb AW, Lee TY: Dynamic CT measurement of cerebral blood flow: A validation study. AJNR: American Journal of Neuroradiology (submitted June, 1998).

Craen, RA: Personal Communication, 1998.

Craen RA, Gelb AW, Murkin JM, Chong KY: CO2 responsiveness of cerebral blood flow is maintained during propofol anaesthesia. Canadian Journal of Anaesthesia 39:A7, 1992.

Dewitt DS, Fatouros PP, Wist AO, et al.: Stable xenon versus radiolabeled microsphere cerebral blood flow measurements in baboons. Stroke 20:1716-1723, 1989.

Eger EI: Isoflurane. A compendium and reference, 2nd Edition. Madison, Anaquest, 1985.

Endo H, Larsen B, Lassen NA: Regional cerebral blood flow alterations remote from the site of intracranial tumors. J Neurosurg 46:271-281, 1977.

Farrell CL: The microcirculation in a glioma model. PhD Thesis, University of Western Ontario, 1988.

Fenstermacher J, Blasberg R, Patlak C: Methods for quantifying the transport of drugs across the brain barrier systems. Pharmacol Ther 14: 217-248, 1981.

Fike JR, Cann CE, Berninger WH: Quantitative evaluation of the canine brain using computed tomography. J Comput Assist Tomogr 6:325-333, 1982.

Furlan A, Kanoti G: When is thrombolysis justified in patients with acute ischemic stroke? A bioethical perspective. Stroke 11:214-218, 1997.

Gamel J, Rousseau WF, Katholi CR, Mesel E: Pitfalls in digital computation of the impulse response of vascular beds from indicator dilution curves. Circ Res 32:516-523, 1973.

Gelb AW, Zhang C, Hamilton JT: Propofol induces dilation and inhibits constriction in guinea pig basilar arteries. Anesth Analg 83:472-476, 1996.

Gill PE, Murray W: Quasi-Newton methods for linearly constrained optimization. In: Gill PE and Murray W (eds), Numerical Methods for Constrained Optimization, pp. 67-92. London, England: Academic Press, 1974.

Gill PE, Murray W: Minimization subject to bounds on the variables. Report NAC 72. London, England: National Physics Laboratory, 1976.

Gobbel GT, Cann CE, Iwamoto HS, Fike JR: Measurement of regional cerebral blood flow in the dog using ultrafast computed tomography. Experimental Validation. Stroke 22:772-779, 1991.

Goldman H: Techniques for measuring cerebral blood flow. In: Phillis JW, ed. The Regulation of Cerebral Blood Flow. Boca Raton: CRC Press Inc., 1993.

Grubb RL, Raichle ME, Eichling JO: The effects of changes in PaCO2 on cerebral blood volume, blood flow, and vascular mean transit time. Stroke 5: 636-37, 1974.

Hamberg LM, Hunter GJ, Halpern EF, Hoop B, Gazelle GS, Wolf GL: Quantitative high-resolution measurement of cerebrovascular physiology with slip-ring CT. AJNR Am J Neuroradiol 17:639-650, 1996.

Harper AM: Physiological control of the cerebral circulation. In: Harper AM, Jennett S, eds. Cerebral Blood Flow and Metabolism, pp. 4-26. Manchester: Manchester University Press, 1990.

Heart and Stroke Facts: 1994 Statistical Supplement. Dallas, Texas: American Heart Association; 1994.

Heymann MA, Payne BD, Hoffman JI, Rudolph AM: Blood flow measurements with radionuclide-labeled particles. Prog Cardiovasc Dis 20:55-79, 1977.

Howard VL: X-ray CT Measurement of Cerebral Blood Volume. MSc Thesis, University of Western Ontario, 1996.

Huda W, Sandison GA: Estimates of the effective dose equivalent, HE, in positron emission tomography studies. Eur J Nucl Med 17:116-120, 1990.

Huda W, Sandison GA: The use of the effective dose equivalents, HE, for 99mTc labelled radiopharmaceuticals. Eur J Nucl Med 1989;15:174-179.

Johnson JD, Young B: Demographics of brain metastasis. Neurosurgery Clinics of North America 7(3): 337-344, 1996.

Knight R, Dereski M, Helpern J, Ordidge R, Chopp M: Magnetic resonance imaging assessment of evolving focal cerebral ischemia. Stroke 25:1252-1262, 1994.

Kucharczyk J, Roberts T, Moseley ME, Watson A: Contrast-enhanced perfusion-sensitive MR imaging in the diagnosis of cerebrovascular disorders. J Magn Reson Imaging 3:241-245, 1993.

Lapin GD, Munson RJ, Groothius DR: Noinvasive CT determination of arterial blood concentration of meglumine iothalamate. J Comput Assist Tomogr 17:108-114, 1993.

Lo EH, Rogowska J, Batchelder KF, Wolf GL: Hemodynamical alterations in focal cerebral ischemia: temporal correlation analysis for functional imaging. Neurol Res 18:150-156, 1996.

Meier P, Zierler KL: On the theory of the indicator-dilution method for measurement of blood flow and volume. J Appl Physiol 6:731-744, 1954.

Miller JD, Bell BA: Cerebral blood flow variations with perfusion pressure and metabolism. In: Wood JH, ed. Cerebral Blood Flow: Physiologic and Clinical Aspects, pp. 119. U.S.A.: McGraw-Hill,1987.

Morris TW, Fischer HW: The pharmacology of intravascular radiocontrast media. Ann Rev Pharmacol Toxicol 26:143-160, 1986.

Nagata K, Asano T: Functional image of dynamic computed tomography for the evaluation of cerebral hemodynamics. Stroke 21:882-889, 1990.

NINDS t-PA Stroke Study Group: Generalized efficacy of t-PA for acute stroke: Subgroup analysis of the NINDS t-PA stroke trial. Stroke 28:2119-2125, 1997.

Palvolgyi R: Regional Cerebral Blood Flow in Patients with Intracranial Tumors. J Neurosurg 31:149-163, 1969.

Patel PM, Mutch WAC: The cerebral pressure-flow relationship during 1.0 MAC isoflurane anesthesia in the rabbit: The effect of different vasopressors. Anesthesiology 72:118-124, 1990.

Patlak CS, Blasberg RG, Fenstermacher JD: Graphical evaluation of blood-to-brain transfer constants from multiple-time uptake data. J Cereb Blood Flow Metab 3: 1-7, 1983.

Patlak CS, Blasberg RG: Graphical evaluation of blood-to-brain transfer constants from multiple-time uptake data. Generalizations. J Cereb Blood Flow Metab 5: 584-590, 1985.

Paulson OB, Strandgaard S, Edvinsson L: Cerebral Autoregulation. Cerebrovasc Brain Metab Rev 2:161-192, 1990.

Penn RK, Walser R, Ackerman L: Cerebral blood volume in man. JAMA 234: 1154-1155, 1975.

Roberts GW, Larson KB: The interpretation of mean transit time measurements for multi-phase tissue systems. J Theor Biol 39:447-475, 1973.

Rosen BR, Belliveau JW, Chien D: Perfusion imaging by nuclear magnetic resonance. Magn Reson Q 5:263-281, 1989.

Scheller MS, Todd MM, Drummond JC: Isoflurane, Halothane, and regional cerebral blood flow at various levels of PaCO2 in rabbits. Anesthesiology 64:598-604, 1986.

Scheller MS, Todd MM, Drummond JC, Zornow MH: The intracranial pressure effects of isoflurane and halothane administered following cryogenic brain injury in rabbits. Anesthesiology 67:507-512, 1987.

Scremin OU, Sonnenschein RR, Rubinstein EH: Cerebrovascular anatomy and blood flow measurements in the rabbit. J Cereb Blood Flow Metab 2(1): 55-66, 1982.

Singal RK, Lee TY, Razvi HA, Mosalei H, Denstedt JD, Chun SS, Bennett J, Romano W, Toll M: Evaluation of Doppler Ultrasonography and Dynamic Contrast-Enhanced CT in Acute and Chronic Renal Obstruction. J Endourol 11:5-11, 1997.

St. Lawrence KS, Lee TY: An Adiabatic Approximation to the Tissue Homogeneity Model for Water Exchange in the Brain. Theoretical Derivation. J Cereb Blood Flow Metab (in press), 1998.

Statistics Canada: Cancer in Canada (Annual). Health Statistics Division, Statistics Canada, 1998.

Steiger HJ, Aaslid R, Stooss R: Dynamic computed tomography imaging of regional cerebral blood flow and blood volume. A clinical pilot study. Stroke 24:591-597, 1993.

Stephan H, Sonntag H, Schenk HD, Kohlhausen S: Effect of Disoprivan (propofol) on the circulation and oxygen consumption of the brain and CO2 reactivity of brain vessels in the human. Anaesthesist 36:60-65, 1987.

Stevens LL: An in-vivo study of angiogenesis in a brain tumour model by dynamic contrast-enhanced CT scanning. MSc Thesis, University of Western Ontario, 1997.

Takahashi JA, Llena JF, Hirano A: Pathology of cerebral metastases. Neurosurgery Clinics of North America 7(3): 345-363, 1996.

Thapar K, Rutka JT, Laws ER: Brain edema, increased intracranial pressure, vascular effects, and other epiphenomena of human brain tumors. In: Kaye AH, Laws ER, eds. Brain Tumors, pp. 163-189. New York, U.S.A: Churchill Livingstone, 1995.

Todd MM, Wu B, Warner DS, Maktabi M: The dose-related effects of nitric oxide synthase inhibition on cerebral blood flow during isoflurane and pentobarbital anesthesia. Anesthesiology 80:1128-1136, 1994.

Tyrrell P: Tomographic measurement of cerebral blood flow and metabolism with positron emitting isotopes in man. In: Harper AM, Jennett S, eds. Cerebral Blood Flow and Metabolism, pp. 90-107. Manchester: Manchester University Press, 1990.

Weeks JB, Todd MM, Warner DS, Katz J: The influence of halothane, isoflurane, and pentobarbitol on cerebral plasma volume in hypocapnic and normocapnia rats. Anesthesiology 73:461-466, 1990.

Yeung IWT, Lee T-Y, Del Maestro RF, Kozak R, Bennet JB, Brown T: An Absorptiometry Method for the Determination of Arterial Blood Concentration of Injected Iodinated Contrast Agent. Phys Med Biol 37:1741-1758, 1992.

Yeung WT, Lee T-Y, Del Maestro RF, Kozak R, Bennett J, Brown T: Effect of steroids on iopamidol blood-brain transfer constant and plasma volume in brain tumors measured with X-ray computed tomography. J Neuro-Oncol 18: 53-60, 1994.

Yonas H: Cerebral Blood Flow Measurement with Stable Xenon-Enhanced Computed Tomography. New York, NY: Raven Press; 1992.

Young WL, Ornstein E: Cerebral and Spinal Cord Blood Flow. In: Cottrrell JE, Smith DS, eds. Anesthesia and Neurosurgery. St. Louis, MO, U.S.A.: Mosby-Year Book, 1994.

Zagzag D, Brem S, Robert F: Neovascularization and tumor growth in the rabbit brain. A model for experimental studies of angiogenesis and the blood-brain barrier. Am J Pathol 131(2): 361-372, 1988.

Zilka E, Ladurner G, Iliff LD, Du Boulay GH, Marshall J: Computer subtraction in regional cerebral blood volume measurements using the EMI-scanner. Br J Radiol 49: 330-334, 1976.

# APPROVED ANIMAL PROTOCOLS

COPY

*September 21, 1995*

*Dear Dr. Gelb:*

*Your "Application to Use Animals for Research or Teaching" entitled:*

*"The Effects of Anaesthetics and Hyperventilation on Cerebral Blood Flow and Cerebral Blood Volumes in Rabbits with Brain Tumors"*
*Funding Agency: Canadian Anaesthetists Society*

*has been approved by the University Council on Animal Care. This approval expires in one year on the last day of the month. The number for this project is # 95207-10. This replaces #94245-10.*

1. *This number must be indicated when ordering animals for this project.*
2. *Animals for other projects may not be ordered under this number.*
3. *If no number appears on this approval please contact this office when grant approval is received. If the application for funding is not successful and if you wish to proceed with the project, request that an internal scientific peer review be performed by your animal care committee.*
4. *Purchases of animals other than through this system must be cleared through the ACVS office. Health certificates will be required.*

*ANIMALS APPROVED*

***NZW Rabbits*** - *16*

*REQUIREMENTS/COMMENTS*

*Please ensure that individual(s) performing procedures, as described in this protocol, are familiar with the contents of this document.*

c.c. ***Approved Renewal*** - *A. Gelb, P. Schoffer, P. Coakwell*
***Approval Letter*** - *P. Schoffer, P. Coakwell*

COPY

October 17, 1996

Dear Dr. Crean, Dr. Gelb, and Dr. Lee:

Your "Application to Use Animals for Research or Teaching" entitled:

"The Effects of Anaesthesia and Hyperventilation on CBV and CBF in Rabbits with Brain Tumors"
Funding Agency: CAS

has been approved by the University Council on Animal Care. This approval expires in one year on the last day of the month. The number for this project is # 96230-10. This replaces #95207-10.

1. This number must be indicated when ordering animals for this project.
2. Animals for other projects may not be ordered under this number.
3. If no number appears on this approval please contact this office when grant approval is received. If the application for funding is not successful and if you wish to proceed with the project, request that an internal scientific peer review be performed by your animal care committee.
4. Purchases of animals other than through this system must be cleared through the ACVS office. Health certificates will be required.

ANIMALS APPROVED

Rabbits - NZW, 3.0-3.5 kg, M - 10

REQUIREMENTS/COMMENTS

Please ensure that individual(s) performing procedures, as described in this protocol, are familiar with the contents of this document.

c.c. Approval Renewal - R. Crean, A. Gelb, T. Lee, S. Henderson, P. Cockwell (6/1/97)
Approval Letter - S. Henderson, K. Perry, P. Cockwell (6/1/97)

*September 21, 1995*

*Dear Dr. Gelb:*

*Your "Application to Use Animals for Research or Teaching" entitled:*

*"C.T. Functional Imaging"*
*Funding Agency: MRC*

*has been approved by the University Council on Animal Care. This approval expires in one year on the last day of the month. The number for this project is # 95206-10. This replaces #94245-10.*

1. *This number must be indicated when ordering animals for this project.*
2. *Animals for other projects may not be ordered under this number.*
3. *If no number appears on this approval please contact this office when grant approval is received. If the application for funding is not successful and if you wish to proceed with the project, request that an internal scientific peer review be performed by your animal care committee.*
4. *Purchases of animals other than through this system must be cleared through the ACVS office. Health certificates will be required.*

*ANIMALS APPROVED*

***NZW Rabbits - 36***

*REQUIREMENTS/COMMENTS*

*Please ensure that individual(s) performing procedures, as described in this protocol, are familiar with the contents of this document.*

c.c. *Approved Renewal - A. Gelb, P. Schoffer, P. Coakwell*
*Approval Letter - P. Schoffer, P. Coakwell*

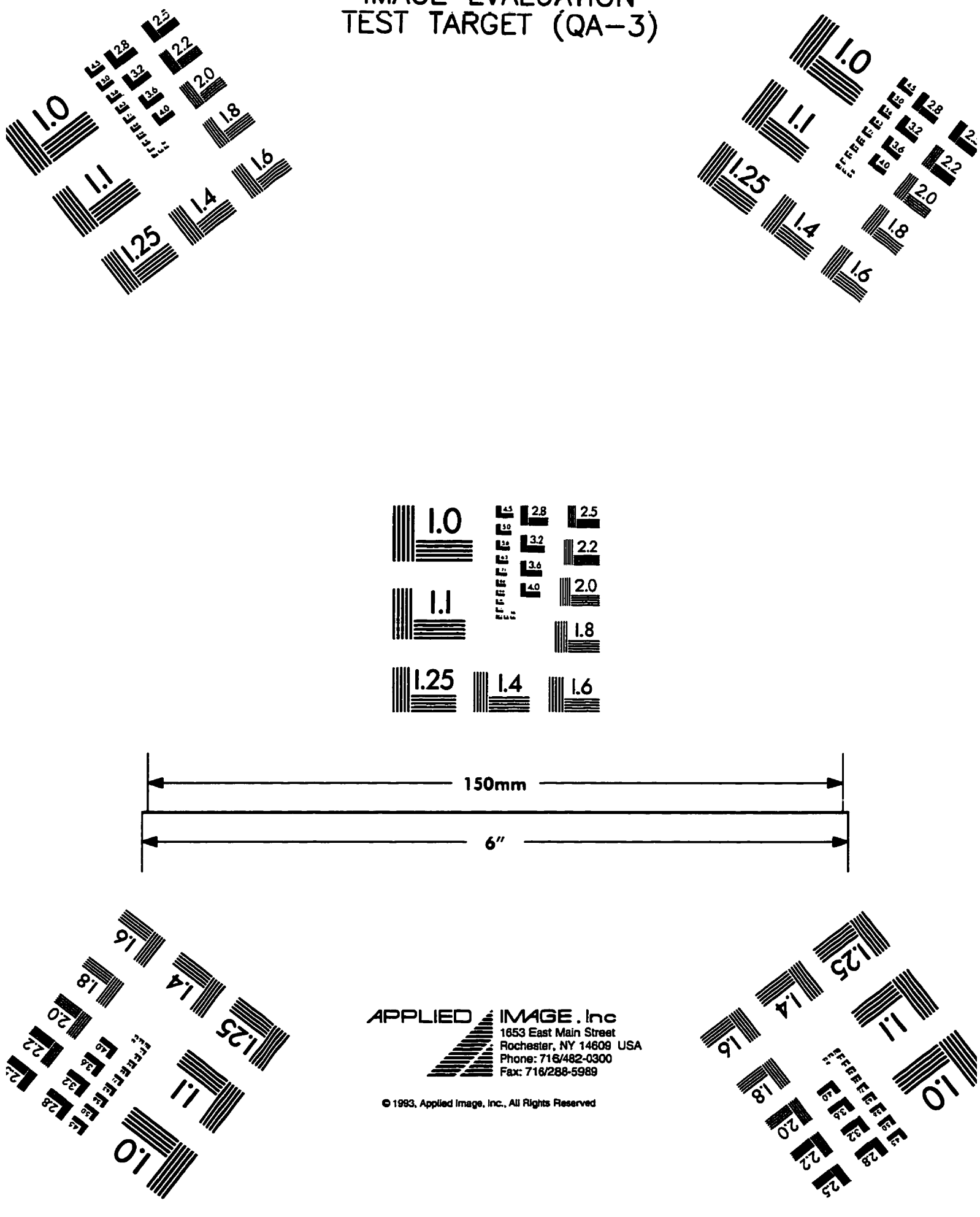
IMAGE EVALUATION
TEST TARGET (QA-3)
1.0
1.1
1.25
1.4
1.6
1.8
2.0
2.2
2.5
2.8
3.2
3.6
4.0
150mm
6"
APPLIED IMAGE, Inc
1653 East Main Street
Rochester, NY 14609 USA
Phone: 716/482-0300
Fax: 716/288-5989
© 1993, Applied Image, Inc., All Rights Reserved